









ARTICLE

# Nucleobindin-1 regulates ECM degradation by promoting intra-Golgi trafficking of MMPs

Natalia Pacheco-Fernandez<sup>1</sup>, Mehrshad Pakdel<sup>1</sup>, Birgit Blank<sup>2</sup>, Ismael Sanchez-Gonzalez<sup>3</sup>, Kathrin Weber<sup>4</sup>, Mai Ly Tran<sup>1,2</sup>, Tobias Karl-Heinz Hecht<sup>1,2</sup>, Renate Gautsch<sup>1</sup>, Gisela Beck<sup>1</sup>, Franck Perez<sup>5</sup>, Angelika Hausser<sup>3</sup>, Stefan Linder<sup>4</sup>, and Julia von Blume<sup>1,2</sup>

**Matrix metalloproteinases (MMPs) degrade several ECM components and are crucial modulators of cell invasion and tissue organization. Although much has been reported about their function in remodeling ECM in health and disease, their trafficking across the Golgi apparatus remains poorly understood. Here we report that the cis-Golgi protein nucleobindin-1 (NUCB1) is critical for MMP2 and MT1-MMP trafficking along the Golgi apparatus. This process is Ca<sup>2+</sup>-dependent and is required for invasive MDA-MB-231 cell migration as well as for gelatin degradation in primary human macrophages. Our findings emphasize the importance of NUCB1 as an essential component of MMP transport and its overall impact on ECM remodeling.**

## Introduction

Organogenesis, growth, and physiological tissue turnover require constant rearrangement and degradation of ECM proteins (Apte and Parks, 2015; Theocharis et al., 2019). For these purposes, human cells secrete a wide variety of different proteases, among which matrix metalloproteinases (MMPs) have been identified as a major group promoting ECM turnover (Kessenbrock et al., 2010; Jobin et al., 2017).

MMPs are Zn<sup>2+</sup>-dependent proteases that degrade various ECM components, such as collagen, gelatin, and fibronectin (Endo et al., 2003; Khokha et al., 2013; Cui et al., 2017). To date, 23 MMPs have been described in humans, which can be grouped into different families based on their substrate specificity (Cui et al., 2017). For instance, MMP2, a well-studied member of the family of gelatinases, is involved in endothelial transmigration, angiogenesis, inflammatory responses, and cancer metastasis (Reichel et al., 2008; Vandooren et al., 2013; Könnecke and Bechmann, 2013; Bonnans et al., 2014; Hannocks et al., 2019).

To ensure proper functioning of these critical processes, the activity of all MMPs is meticulously controlled. All MMPs except MMP23 share a basic structure, with three domains designated as propeptide, catalytic, and hemopexin (Fig. 1 A; Cui et al., 2017). The propeptide is crucial for MMP activation because it contains a “cysteine switch” motif in which cysteine binds to the Zn<sup>2+</sup> ion of the catalytic pocket. Once this linkage is cleaved, the catalytic pocket is accessible and the MMP becomes active (Tallant et al., 2010; Cui et al., 2017; Alaseem et al., 2019). For MMP2, this activation step occurs mainly at the plasma membrane and is mediated by membrane type 1 (MT1)-MMP, a

membrane-bound protein of the same family that, in conjunction with tissue inhibitor of metalloproteinase 2 (TIMP2), cleaves the propeptide domain (Fernandez-Catalan et al., 1998; Brew and Nagase, 2010; Han et al., 2015). This interplay between MT1-MMP and MMP2 is the main step in invasive cell migration and ECM proteolysis, as shown by previous studies that have demonstrated their accumulation at characteristic proteolytic adhesion spots, such as podosomes in myeloid cells and invadopodia in cancer cells (Van Goethem et al., 2010; Jacob et al., 2013; Shaverdashvili et al., 2014; Han et al., 2015; Linder and Wiesner, 2015).

Soluble and membrane-associated MMPs are synthesized as inactive precursors (zymogens) in the ER and then transported to the Golgi apparatus, as described for other cargoes of the secretory pathway (Barlowe and Miller, 2013; McCaughey and Stephens, 2018). Upon reaching the Golgi, they are sorted and transported to specific membrane domains at the cell surface (Deryugina et al., 2004; Kean et al., 2009; Frittoli et al., 2014; Kajiho et al., 2016). Thus far, several cytosolic factors such as microtubules and motor proteins as well as Rab GTPases are considered necessary for MMP transport (Sbai et al., 2010; Wiesner et al., 2010, 2013; Gueye et al., 2011; Frittoli et al., 2014; Linder and Scita, 2015; Jacob et al., 2016).

The divalent ion calcium (Ca<sup>2+</sup>) is a key component of the reaction by which secretory cargoes are sorted and packed for transport out of the Golgi apparatus (Porat and Elazar, 2000; Ton and Rao, 2004; Pizzo et al., 2010; Lissandron et al., 2010; Rayl et al., 2016; Margulis et al., 2016). Recent studies have

<sup>1</sup>Max Planck Institute of Biochemistry, Martinsried, Germany; <sup>2</sup>Department of Cell Biology, Yale University School of Medicine, New Haven, CT; <sup>3</sup>Institute of Cell Biology and Immunology, University of Stuttgart, Stuttgart, Germany; <sup>4</sup>Institut für Medizinische Mikrobiologie, Virologie und Hygiene, Universitätsklinikum Hamburg, Hamburg, Germany; <sup>5</sup>Institute Curie, PSL Research University, Centre National de la Recherche Scientifique, UMR 144, Paris, France.

Correspondence to Julia von Blume: [julia.vonblume@yale.edu](mailto:julia.vonblume@yale.edu).

© 2020 Pacheco-Fernandez et al. This article is distributed under the terms of an Attribution–Noncommercial–Share Alike–No Mirror Sites license for the first six months after the publication date (see <http://www.rupress.org/terms/>). After six months it is available under a Creative Commons License (Attribution–Noncommercial–Share Alike 4.0 International license, as described at <https://creativecommons.org/licenses/by-nc-sa/4.0/>).

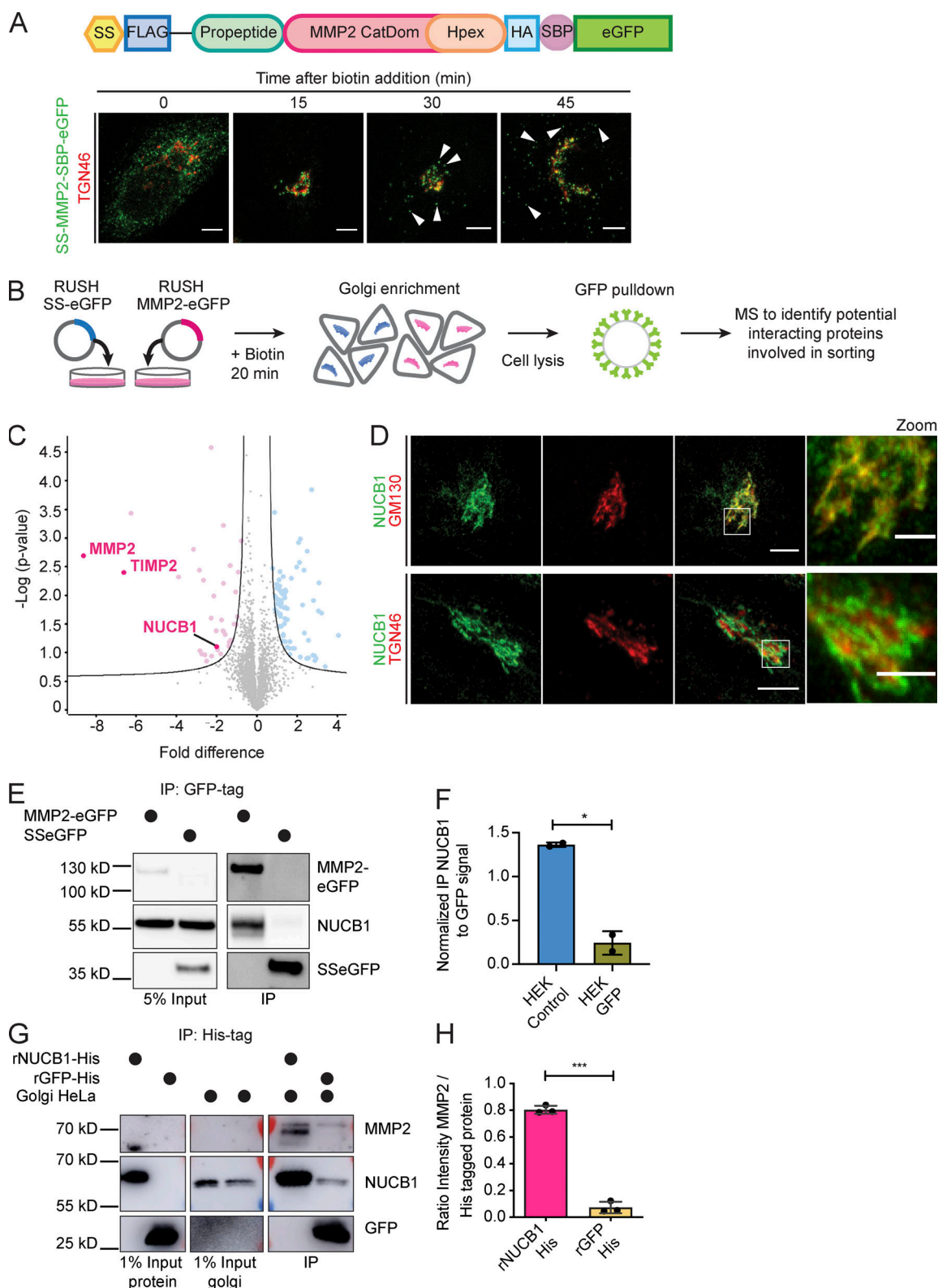


**Figure 1. Identification of candidates involved in the trafficking of MMP2.** (A) Scheme of the MMP2 RUSH construct. SS-Flag-MMP2-HA-SBP-eGFP was used as a reporter. Fluorescence images show HeLa cells expressing MMP2-SBP-eGFP counterstained against TGN46 (red). Without biotin, MMP2 is retained in the ER (0 min). It reaches the Golgi 15 min after biotin addition and is sorted into vesicles (arrowheads) at 30 and 45 min, respectively. Scale bars, 5  $\mu$ m. (B) MS strategy to identify MMP2 interacting partners in the Golgi. HeLa cells expressing MMP2-SBP-eGFP or SS-SBP-eGFP were incubated for 20 min with biotin to enrich reporter proteins at the Golgi. After GFP IP, samples were analyzed using MS ( $n = 3$ ). (C) Volcano plot highlights significantly enriched MMP2 interactors in pink. 42 sorting-related candidates were found, among them TIMP2, a known inhibitor of MMP2, and NUCB1. Two-sample  $t$  test, false discovery rate = 0.3, minimum fold change = 0.5. (D) Fluorescence images of HeLa cells labeled with endogenous NUCB1 (green) and GM130 or TGN46 (red). Scale bars, 5  $\mu$ m;

zoom, 2  $\mu$ m. (E) HEK 293T cells expressing SS-MMP2-SBP-eGFP or SS-SBP-eGFP were processed for GFP IP and WB analysis. (F) Semiquantitative analysis of the normalized NUCB1 to GFP signal from two independent experiments. Significance: one-sample *t* test. (G) His-tag coIP of recombinant rNUCB1-His. Endogenous MMP2 from HeLa Golgi membranes coimmunoprecipitated with rNUCB1-His but not rGFP-His. (H) Semiquantitative analysis of the MMP2 signal from three independent experiments. Bars, mean  $\pm$  SD. Paired *t* test: \*, *P* < 0.05; \*\*\*, *P* < 0.001.

revealed the molecular mechanisms by which  $\text{Ca}^{2+}$ -based cargo sorting and export occur at the Golgi (Micaroni et al., 2010; Deng et al., 2018). In this regard, Cab45, a soluble  $\text{Ca}^{2+}$ -binding protein, acts on local, transient  $\text{Ca}^{2+}$  influx at the trans-Golgi network (TGN). After mediated influx by  $\text{Ca}^{2+}$  ATPase SPCA1, Cab45 assembles into oligomers and sorts secretory cargoes into sphingomyelin-rich transport carriers (von Blume et al., 2011, 2012; Crevenna et al., 2016; Deng et al., 2018).

Human cells express another luminal Golgi  $\text{Ca}^{2+}$ -binding protein called nucleobindin-1 (NUCB1), which, in contrast to Cab45, localizes to the cis-Golgi compartment (Lin et al., 1998, 1999; Lavoie et al., 2002; Tulke et al., 2016). Earlier studies have postulated NUCB1 to be a regulator of endosomal recycling of lysosomal receptors (Brodeur et al., 2009; Larkin et al., 2016); however, whether NUCB1 has a role in the anterograde intra-Golgi (IG) transport of proteins is unknown.

Here we identify NUCB1 as an MMP2 binding partner and show that NUCB1 is required for its trafficking through the Golgi apparatus. The functional association of MMP2 and NUCB1 occurs in the lumen of the cis-Golgi compartment in a  $\text{Ca}^{2+}$ -dependent manner and is required for MMP2 and MT1-MMP trafficking through the Golgi. We provide further evidence that NUCB1 silencing perturbs ECM degradation in human primary macrophages, as well as MMP-dependent ECM degradation and invasive cell migration in MDA-MB-231 cells, highlighting the physiological relevance of NUCB1 in MMP2 and MT1-MMP trafficking. Our study provides insight into the molecular mechanisms underlying MMP IG transport and identifies NUCB1 as a central regulator of protein trafficking at the cis-Golgi.

## Results

### Visualization of MMP2 trafficking in living cells

The “retention using selective hooks” (RUSH) system was used to investigate MMP2 trafficking (Boncompain et al., 2012). This system allows quantitative analysis of the secretory pathway by synchronous release of cargo, which is achieved at a physiological temperature using biotin (Boncompain et al., 2012). We generated an MMP2 construct C-terminally tagged with streptavidin binding peptide (SBP) followed by an enhanced green fluorescent protein (eGFP) to obtain the fusion protein signal sequence (SS)-MMP2-SBP-eGFP as a reporter, whereas streptavidin tagged KDEL was used as an ER retention hook (Fig. 1 A). Confocal microscopy images show that in the absence of biotin, MMP2 localized to the ER. Upon 15 min of biotin incubation, MMP2 reached the Golgi and localized to secretory vesicles after 30 and 45 min (Fig. 1 A). We also confirmed that MMP2-eGFP is actually secreted from cells by staining the released protein with an anti-GFP antibody (Fig. S1 A). Furthermore, we costained MMP2-GFP vesicles with Rab5, Rab6, Rab7, Rab8, Rab11, mCherry lysosomes, and Lysozyme C (LyzC)-mCherry (Fig. S2).

MMP2 containing TGN-derived vesicles did not overlap with any of these endosomal, lysosomal, or Rab GTPase markers. Nevertheless, MMP2 TGN-derived vesicles partially colocalized with LyzC, a protein sorted into sphingomyelin-rich vesicles. Hence, the RUSH assay robustly monitors MMP2 trafficking through the secretory pathway.

### Identification of novel interaction partners controlling MMP2 trafficking

To gain insight into the molecular mechanism of MMP2 trafficking, we implemented a novel proteomics approach to identify endogenous interacting proteins involved in protein transport (Fig. 1 B). HeLa cells expressing either SS-MMP2-SBP-eGFP or SS-SBP-eGFP were incubated for 20 min with biotin to enrich the reporter proteins at the Golgi, subjected to GFP immunoprecipitation (IP), and analyzed by mass spectrometry (MS, Fig. 1 B). We identified 42 interacting proteins significantly enriched in SS-MMP2-SBP-eGFP IPs (Table S1 and Fig. 1 C). MMP2 and a widely described interacting protein (TIMP2) were significantly enriched, validating our results (Fig. 1 C). Furthermore, NUCB1, an EF-hand domain (EFh)  $\text{Ca}^{2+}$ -binding protein that localizes to the cis-Golgi and is considered to be its major luminal  $\text{Ca}^{2+}$  regulator, was identified. NUCB1 and Cab45 share several similarities, as both are luminal  $\text{Ca}^{2+}$  resident proteins in the Golgi and belong to the same EFh protein family. Given that Cab45 has been described as crucial in  $\text{Ca}^{2+}$ -dependent sorting of soluble secretory proteins (von Blume et al., 2012; Crevenna et al., 2016; Deng et al., 2018), we focused on elucidating the role of NUCB1 in MMP2 trafficking.

### NUCB1 interacts with MMP2 at the Golgi

We first corroborated the reported localization of NUCB1 in HeLa cells by costaining endogenous NUCB1 with the cis- and trans-Golgi markers GM130 and TGN46, respectively (Fig. 1 D). Colocalization with GM130 but not with TGN46 indicates a cis-Golgi localization, in agreement with previous reports (Lin et al., 1998). Based on the MS results, we performed IP experiments to verify the interaction of MMP2 with NUCB1 (Fig. 1 E). To this end, HEK293T cells expressing SS-MMP2-SBP-eGFP or SS-SBP-eGFP were incubated with biotin for 15 min to accumulate MMP2-eGFP or SS-eGFP in the Golgi, and IPs were performed. Western blotting (WB) with GFP and NUCB1 antibodies (Fig. 1 E) evidenced an interaction between endogenous NUCB1 and MMP2-eGFP but not with SS-SBP-GFP (Fig. 1, E and F). To further validate such interaction in the Golgi, we incubated recombinant His-tagged NUCB1 (rNUCB1-His; Fig. S3 A) or GFP (rGFP-His) with detergent-solubilized Golgi membranes purified from HeLa cells (von Blume et al., 2012). Ni-NTA pull-downs showed endogenous MMP2 coIP with rNUCB1-His, but not with rGFP-His (Fig. 1, G and H).

To better characterize the interaction between NUCB1 and MMP2, we generated purified recombinant His-SUMO-MMP2



(rHS-MMP2; Fig. S3, B and C) and performed analytical ultracentrifugation (AUC), a technique that shows sedimentation of macromolecules in solution. For this experiment, rHS-MMP2 was bioconjugated with Cy3 via maleimide labeling and analyzed by AUC. As expected, the sedimentation peak of rHS-MMP2-Cy3 occurred at 4.705 S (measured Stokes radius at 20°C: 4.41 nm), and the calculated molecular weight was ~87.1 kD (Fig. S3 D). Then, we evaluated the AUC profiles of rHS-MMP2-Cy3 and rNUCB1-His in solution (Fig. S3 E), finding a peak at 3.189 S that indicates a shift in the sedimentation velocity and is associated with a direct interaction between NUCB1 and MMP2 (Stokes radius at 20°C: 8.41 nm). The calculated molecular weight was 112 kD, close to the theoretical molecular weight of the complex (Fig. S3 E). Altogether, these data confirmed that NUCB1 interacts with MMP2 in the Golgi.

### MMP2 trafficking is delayed in NUCB1 knockout (KO) cells

Next, we generated NUCB1-KO HeLa cells using CRISPR/Cas9 and confirmed the KO by WB and immunofluorescence (Fig. S1, B–D). We then analyzed the impact of NUCB1 on MMP2 trafficking by monitoring the transport kinetics of MMP2 at a single-cell level using the RUSH system in control and NUCB1-KO cells (Fig. 2 A). Quantification of SS-MMP2-SBP-eGFP-containing vesicles showed that the median number of vesicles in control cells after 30 min of biotin addition was 29 (interquartile range [IQR], 17–52.75), whereas it was significantly reduced to 8 (IQR, 3–26) in NUCB1-KO cells (Fig. 2 B). Reexpression of NUCB1-WT fully restored the amount of SS-MMP2-SBP-eGFP-positive vesicles to control levels in NUCB1-KO cells (median, 36.5; IQR, 17–51.75; Fig. 2 B).

Previous studies have documented the expression of NUCB1 in the lumen of the Golgi as well as in the cytosol (Brodeur et al., 2009; Kapoor et al., 2010). To confirm that Golgi-localized NUCB1 is exclusively required to rescue the described MMP2 trafficking delay, NUCB1-KO cells were transfected with cytosolic NUCB1 (NUCB1-cyto). Importantly, NUCB1-cyto could not rescue the delay observed in NUCB1-KO cells, further confirming that Golgi-localized NUCB1 is necessary for MMP2 trafficking (Fig. S4, A and B).

To assess the specificity of this defect, we performed RUSH experiments using the Cab45 cargo lysozyme C (LyzC)-eGFP (LyzC-SBP-eGFP; Deng et al., 2018). Cells were imaged at 20, 40, and 60 min after biotin incubation to quantify cytosolic vesicles (Fig. 2 C), showing that NUCB1 depletion does not alter LyzC trafficking (Fig. 2 D). Simultaneously, we monitored Flag-tagged SS-MMP2-SBP-eGFP and SS-LyzC-SBP-eGFP secretion in a pool of control and NUCB1-KO HeLa cells. WB analysis of cell culture supernatants showed reduced secretion of SS-MMP2-SBP-eGFP in NUCB1-KO cells after 45 min of biotin incubation (Fig. 2, E and F); however, no effect was observed for SS-LyzC-SBP-eGFP. To further validate the specificity of NUCB1 and MMP2 binding, we evaluated whether there was an interaction between LyzC-eGFP with NUCB1. Whereas NUCB1 specifically interacted with MMP2, it did not bind to LyzC in HeLa control, NUCB1-KO, or NUCB1-WT reconstituted cells (Fig. 2, G and H).

Moreover, to evaluate whether NUCB1 is required for the trafficking of other members of the MMP family, we analyzed

the trafficking of MT1-MMP (Fig. S4 C). Control and NUCB1-KO cells with or without reexpression of NUCB1-WT were transiently transfected with the RUSH construct SS-MT1-MMP-SBP-mCherry and analyzed at 30, 60, and 90 min after biotin addition (Fig. S4 D). Quantification of SS-MT1-MMP-SBP-mCherry-positive vesicles at 60 min after biotin addition showed a significant reduction in number of vesicles in NUCB1-KO cells (median, 2.5; IQR, 0.25–7) compared with the HeLa control (median, 10; IQR, 4–36; Fig. S4 E). Importantly, reexpression of NUCB1-WT restored the numbers of positive MT1-MMP vesicles to control levels (median, 13; IQR, 7.5–21; Fig. S4 E).

To determine if the trafficking of endogenous MT1-MMP to the cell surface was affected by NUCB1, we performed a cell surface biotinylation assay. Briefly, after HeLa or NUCB1-KO cells were incubated with sulfo-NHS-SS-biotin for 90 min, biotinylated proteins were pulled down using NeutrAvidin beads. WB analysis revealed less endogenous MT1-MMP on the cell surface of NUCB1-KO cells than on HeLa control cells (Fig. S4 F), confirming a defect in the transport of endogenous MT1-MMP to the cell surface (Fig. S4 G).

Taken together, these results indicate that NUCB1 is a specific component for the trafficking of MMP2 and MT1-MMP. Given that MT1-MMP can activate MMP2 at the plasma membrane, we investigated whether reduced secretion of MMP2 could be related to a defect in the surface availability of MT1-MMP. For this purpose, we performed gel zymography of cell culture supernatants from HeLa and NUCB1-KO cells expressing SS-MMP2-SBP-eGFP after 45 min of biotin incubation. We observed no differences in MMP2 activity between NUCB1-KO and HeLa control cells (Fig. S5, A and B), indicating that the differences observed in the secretion phenotype are not caused by an activation defect.

To further investigate the role of NUCB1 in secretory protein trafficking, we analyzed the secretion of SS-HRP in control and NUCB1-KO cells. Similar to LyzC, SS-HRP secretion was not affected by NUCB1-KO (Fig. S5, C and D). We also tested if NUCB1 impacted protein transport to lysosomes by monitoring the trafficking of cathepsin D (cathD). After 20, 40, and 60 min of biotin incubation, confocal microscopy images of control and NUCB1-KO cells expressing SS-SBP-eGFP-cathD revealed no differences in the number of cathD vesicles between these cells, indicating that protein transport to lysosomes was not affected by NUCB1 (Fig. S5, E and F). Overall, our data show that NUCB1 is not a universal regulator of protein trafficking in the secretory pathway, but rather it plays a specific role in MMP2 trafficking.

### NUCB1 facilitates MMP2 IG transport

To better dissect the role of NUCB1 in the trafficking of MMP2, we performed RUSH experiments in control and NUCB1-KO cells costained with ER-Golgi intermediate compartment (ERGIC) and Golgi markers. Early trafficking of MMP2 from the ER to ERGIC was monitored by colocalization of MMP2 and ERGIC-resident 53-kD membrane protein (ERGIC53). After 2.5, 5, and 7.5 min of biotin incubation (Fig. 3 A), Pearson's correlation coefficients (PCs) of MMP2 and ERGIC53 showed no significant differences between control and NUCB1-KO cells, suggesting no traceable MMP2 trafficking defect from ER to Golgi (Fig. 3 B). In

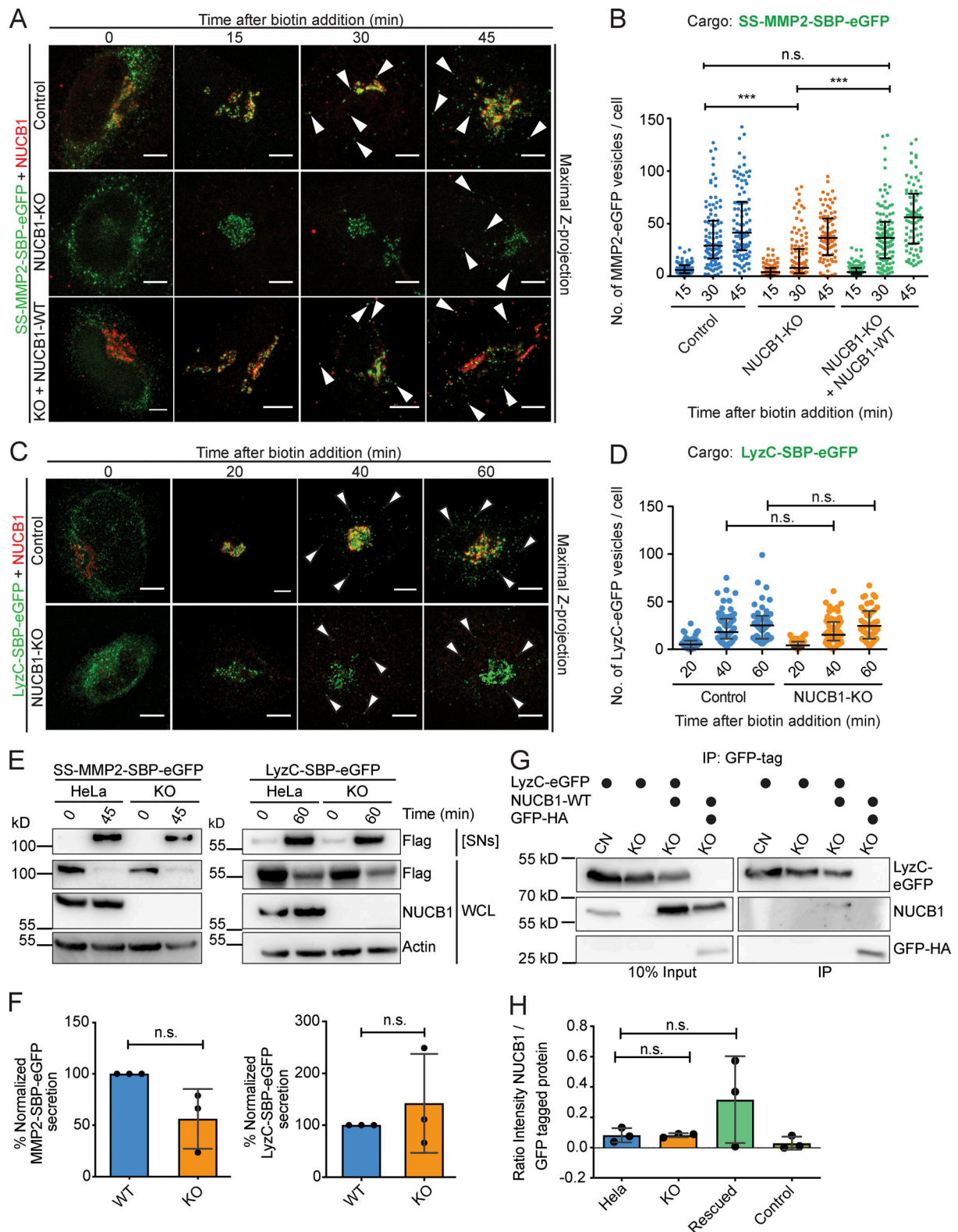


**Figure 2. NUCB1-KO impairs the trafficking of MMP2. (A)** Fluorescent images of HeLa or NUCB1-KO cells expressing SS-MMP2-SBP-eGFP with or without NUCB1-WT, counterstained against NUCB1 (red) and captured after 0, 15, 30, and 45 min of biotin incubation. Arrowheads, cytoplasmic vesicles. Scale bars, 5  $\mu$ m. **(B)** Cytoplasmic vesicle counts as described in A are plotted as number of vesicles per cell ( $n \geq 90$  cells, median  $\pm$  IQR of two independent experiments; \*\*\*,  $P < 0.001$ ; n.s., not significant). **(C)** Confocal microscopy images of HeLa or NUCB1-KO cells expressing LyzC-SBP-eGFP and counterstained against NUCB1 (red) after 0, 20, 40, and 60 min of biotin incubation. Arrowheads, cytoplasmic vesicles. Scale bars, 5  $\mu$ m. **(D)** Cytoplasmic vesicle counts from C of two independent experiments ( $n \geq 42$  cells, median  $\pm$  IQR). **(E)** Secretion assay of HeLa or NUCB1-KO cells expressing SS-MMP2-SBP-eGFP or LyzC-SBP-eGFP and incubated with biotin for 45 or 60 min, respectively. WCL, whole-cell lysates. [SNs], 10 $\times$ -concentrated supernatants. **(F)** Semiquantitative analysis from three

independent experiments, one-sample *t* test. Bars, mean  $\pm$  SD. **(G)** GFP-coIP of HeLa or NUCB1-KO cells expressing LyzC-eGFP, with or without NUCB1-WT. GFP-HA, negative control; CN, HeLa control; KO, NUCB1-KO. **(H)** Semiquantitative analysis of NUCB1 to GFP signal from three independent experiments. Bars, mean  $\pm$  SD; paired *t* test.

contrast, PC quantification of MMP2 with the cis-Golgi marker GM130 (Fig. 3 C) revealed reduced colocalization in NUCB1-KO cells at 10, 15, and 20 min after biotin addition (Fig. 3 D). After 25 and 30 min, MMP2-GM130 colocalization recovered to similar control cell levels, indicating that MMP2 transport is delayed in the absence of NUCB1 at the early stages of the cis-Golgi (Fig. 3 D).

Finally, we analyzed the colocalization of MMP2 with the trans-Golgi marker TGN46 (Fig. 3 E). PC of MMP2 with TGN46 showed significant differences in NUCB1-KO cells only at 20 and 25 min of biotin incubation but not at later time points (Fig. 3 F). Therefore, MMP2 IG trafficking appears to be affected from cis- to trans-Golgi in the absence of

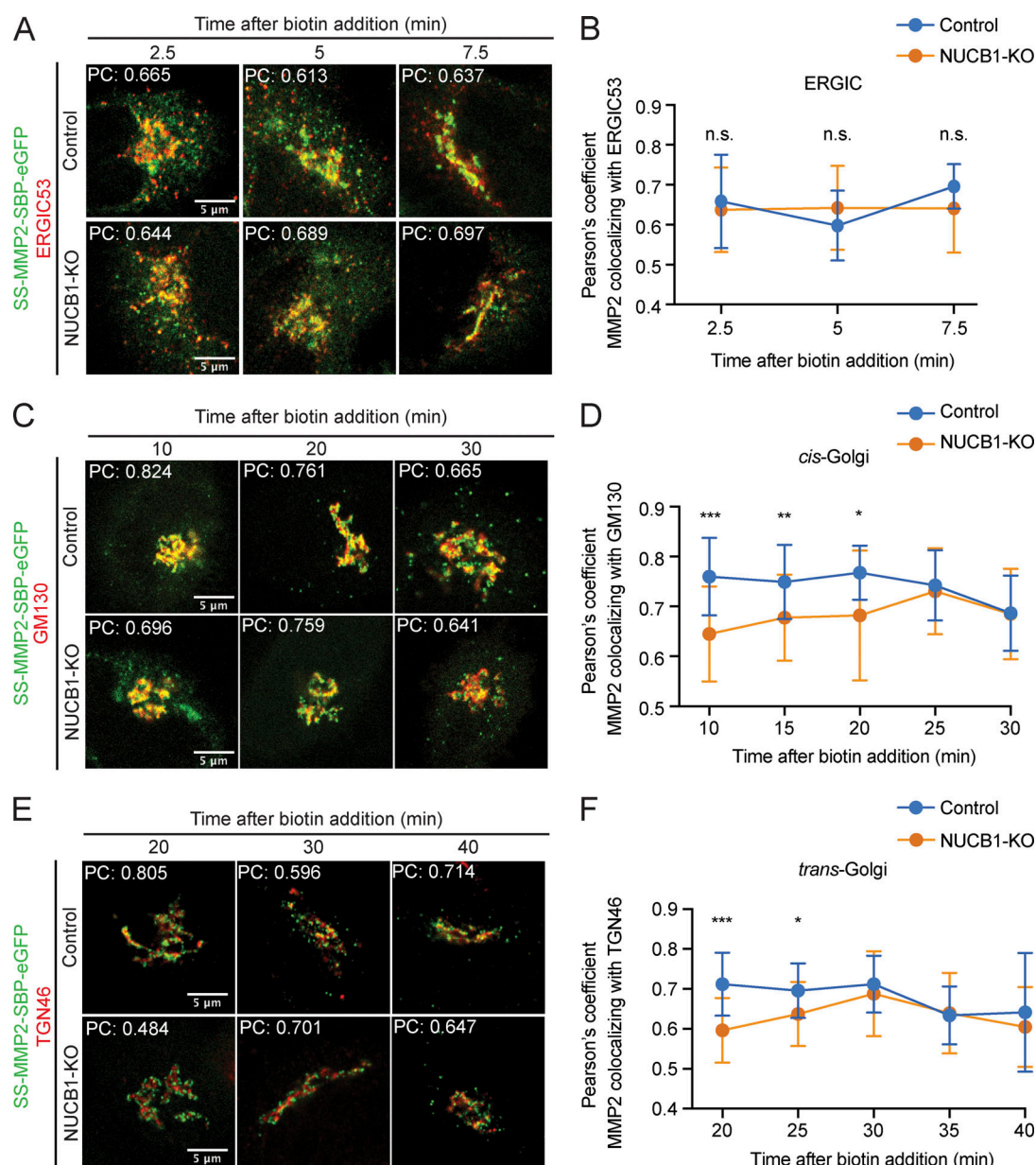


**Figure 3. MMP2 trafficking delay occurs at the cis-Golgi.** **(A)** Fluorescence images of HeLa or NUCB1-KO cells transiently expressing SS-MMP2-SBP-eGFP, fixed at 2.5, 5, and 7.5 min after biotin addition, and counterstained against ERGIC53 (red). Scale bars, 5  $\mu$ m. **(B)** Average PC per time point. **(C)** Colocalization of HeLa or NUCB1-KO cells expressing SS-MMP2-SBP-eGFP with GM130 (red) after 10, 15, 20, and 25 min of biotin incubation. Scale bars, 5  $\mu$ m. **(D)** Average PC illustrates decreased colocalization at 10, 15, and 20 min after biotin addition. **(E)** Colocalization of SS-MMP2-SBP-eGFP with TGN46 (red) expressed in HeLa or NUCB1-KO cells at 20, 25, 30, 35, and 40 min after biotin addition. Scale bars, 5  $\mu$ m. **(F)** Average PC shows that MMP2 is equally colocalizing with TGN46 in HeLa and NUCB1-KO cells upon arrival at the TGN. Error bars represent SD; \*,  $P < 0.05$ ; \*\*,  $P < 0.01$ ; \*\*\*,  $P < 0.001$ ; n.s., not significant.



NUCB1, but not protein sorting into vesicles upon arrival at the TGN.

To further substantiate the trafficking defect observed in NUCB1-KO cells, we performed live-cell wide-field microscopy experiments in cells expressing SS-MMP2-SBP-eGFP after biotin addition (Fig. 4 A). To obtain a better temporal resolution of MMP2 trafficking and sorting into vesicles, we quantified MMP2 vesicles at 1-min time intervals (Fig. 4 B). Within the first 32 min of MMP2 transport after cargo release from the ER, no significant differences were observed in the number of MMP2-containing vesicles between HeLa and NUCB1-KO cells. Interestingly, between 33 and 43 min, MMP2 vesicle numbers were significantly lower in NUCB1-KO cells (Fig. 4 B), supporting our previous findings (Fig. 2, A and B) and indicating that NUCB1 is indeed required for proper MMP2 IG trafficking.

Furthermore, to confirm that the observed delay in NUCB1-KO cells is not due to a defect in ER-to-Golgi transport, we evaluated the arrival of MMP2 to the Golgi over time. Using live-cell time-lapse videos, we evaluated Golgi compaction as a measure of MMP2 kinetics by calculating the Golgi area in each 1-min time frame normalized to the ER area at time 0, i.e., without biotin addition (Fig. 4 C). Within the first 18 min of MMP2 transport, no significant differences between control and NUCB1-KO cells were observed (Fig. 4 D). Between 19 and 26 min, NUCB1-KO cells showed a significant delay in MMP2 trafficking that peaked at 21 min. After this period, MMP2 transport in NUCB1-KO cells was similar to control (Fig. 4 D). These data corroborate our previous results (Fig. 3, A–F) and show that MMP2-eGFP requires more time traveling through the Golgi, suggesting that NUCB1 is specifically required for MMP2 trafficking from the cis-Golgi compartment.

To rule out the “premature” export of SS-MMP2-SBP-eGFP from the ER, we analyzed its localization before biotin addition in control and NUCB1-KO cells in relation to the ER exit site marker Sec16. Confocal microscopy images showed only partial colocalization between MMP2 and Sec16, and quantification of the colocalization of these proteins showed no significant difference between HeLa control and NUCB1-KO cells, indicating that MMP2 export is similar in both cell lines at ER exit sites (Fig. 4, E and F).

### Ca<sup>2+</sup> binding by NUCB1 is essential for IG trafficking of MMP2

Proteins in the EFh family of Ca<sup>2+</sup>-binding proteins differ in the number of their EFh motifs. For example, Calumenin and Cab45 have 6 EFhs, CaM has 4, and NUCB1 has a single pair (Fig. 5 A; Leung et al., 2019; Honoré and Vorum, 2000; Honoré, 2009). The NUCB1 EFhs show high similarity to EFh 3 of Calumenin, EFhs 3 and 4 of Cab45, and EFhs 1 and 2 of CaM (Lin et al., 1999). As a characteristic feature, a highly conserved glutamic acid residue (E) flanks both EFhs (Miura et al., 1994; Gonzalez et al., 2012). Together with aspartic acid (D), these residues are part of what Lin et al. (1999) described as an ideal EF-hand motif, in which the interaction between the oxide groups of D or E, plus carbonyl groups of the peptide chain and water, constitute the Ca<sup>2+</sup>-binding site. Besides that, previous reports have shown that the EFhs of a recombinant cytosolic version of NUCB1 are essential for its interaction with the  $\alpha$ -subunit of G-protein-coupled receptors (Kapoor et al., 2010).

To investigate the significance of these EFhs for MMP2 binding, we generated a Ca<sup>2+</sup>-binding deficient mutant of NUCB1 (NUCB1-mEFh1+2) by substituting E264 in EFh1 and E316 in EFh2 (Fig. 5 B, dark blue) with a glutamine (Q; Fig. 5 B, pink). Then, we evaluated the relevance of Ca<sup>2+</sup> in the interaction of NUCB1 to MMP2 using GFP IPs of NUCB1-KO cells expressing SS-Flag-MMP2-HA-eGFP (MMP2-eGFP) and reconstituted with NUCB1-WT or NUCB1-mEFh1+2. WB analysis revealed a significant reduction in the interaction between NUCB1 and MMP2 when both EFhs were mutated, indicating that Ca<sup>2+</sup>-binding is crucial for the interaction of NUCB1 with MMP2 (Fig. 5, C and D).

Next, SS-MMP2-SBP-eGFP was expressed in control, NUCB1-KO, and NUCB1-KO cells reconstituted with either NUCB1-WT or NUCB1-mEFh1+2 (Fig. 5 E), to evaluate if Ca<sup>2+</sup> binding impacts MMP2 trafficking. The number of MMP2-eGFP-positive vesicles in NUCB1-KO and NUCB1-EFh1+2-expressing cells was significantly reduced compared with control cells and NUCB1-WT-reexpressing cells (Fig. 5 F), confirming the essential role of Ca<sup>2+</sup> binding in the trafficking of MMP2.

To assess the role of NUCB1 in Golgi Ca<sup>2+</sup> homeostasis, Ca<sup>2+</sup> influx into the Golgi was monitored using a previously established workflow (Lissandron et al., 2010; von Blume et al., 2011; Kienzle et al., 2014; Deng et al., 2018). To this end, we generated a novel low-affinity Förster resonance energy transfer (FRET)-based Ca<sup>2+</sup> sensor called GPP130-Twitch5, which localized to the cis-Golgi membrane and allowed the measurement of local Ca<sup>2+</sup> uptake.

Ca<sup>2+</sup> uptake was measured by depleting luminal Ca<sup>2+</sup> in control or NUCB1-KO cells expressing GPP130-Twitch5 with ionomycin. Next, Ca<sup>2+</sup> was added, and FRET signals were captured (Fig. 6 A). Cis-Golgi [Ca<sup>2+</sup>] fluorescence signals were normalized to  $\Delta R/R_0$  (see Materials and methods; Deng et al., 2018). After adding 2.2 mM CaCl<sub>2</sub> to the culture medium, fluorescent microscopy images showed a stronger increase in cis-Golgi Ca<sup>2+</sup> levels in control compared with NUCB1-KO cells (Fig. 6 A). Quantification of Ca<sup>2+</sup> influx showed a  $30.0 \pm 8.8\%$  increase in FRET signal in control cells compared with  $16.3 \pm 10.3\%$  in NUCB1-KO cells (Fig. 6 B). Reexpression of NUCB1-WT restored FRET increase to control levels after Ca<sup>2+</sup> addition, whereas expression of NUCB1-EFh1+2 did not (Fig. 6 B). Importantly, defects in Ca<sup>2+</sup> homeostasis were exclusively observed at the cis-Golgi, as the analysis of cells expressing the TGN-localized FRET Ca<sup>2+</sup> sensor Go-D1-cpv (Lissandron et al., 2010) showed no significant differences in Ca<sup>2+</sup> influx into the TGN in NUCB1-KO cells (Fig. 6, C and D). These results demonstrate that NUCB1 depletion or NUCB1 EFh point mutations disrupt Ca<sup>2+</sup> homeostasis specifically in the cis-Golgi but not the TGN.

### NUCB1 modulates invasive cell migration and ECM degradation

Given the relevance of MMP2 in ECM remodeling, we hypothesized that silencing of NUCB1 would have a direct effect on ECM degradation and MMP-dependent invasive migration. To further investigate the role of NUCB1, we transfected invasive human breast adenocarcinoma MDA-MB-231 cells stably expressing MT1-MMP (Sakurai-Yageta et al., 2008) with two different siRNAs for NUCB1 (Fig. 7, A and B) or MMP2 (Fig. 7 C). The secretion of endogenous MMP2 was evaluated in control or

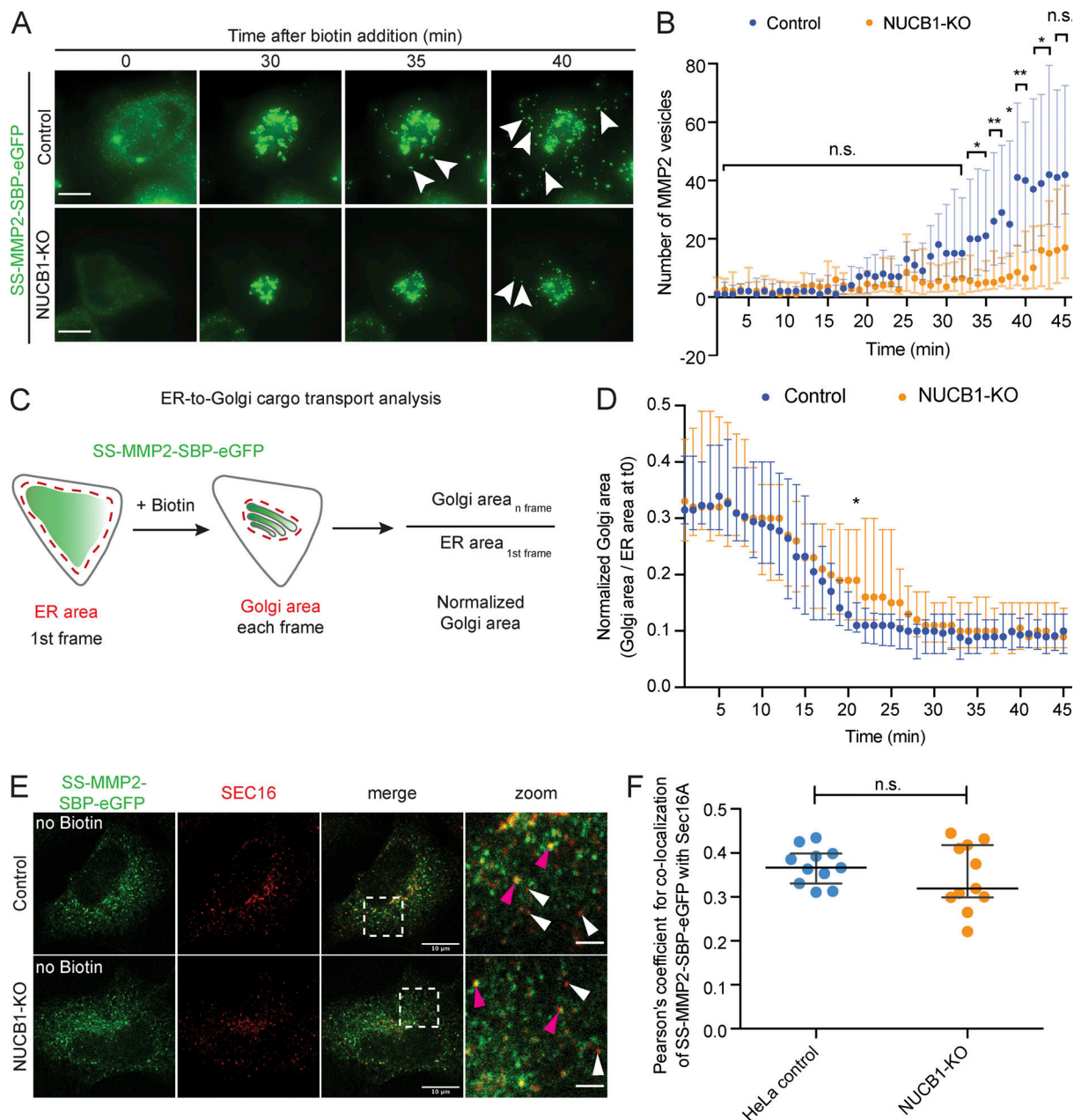


**Figure 4. MMP2 trafficking is exclusively delayed at the Golgi in living cells.** (A) HeLa or NUCB1-KO cells expressing SS-SBP-MMP2-eGFP were analyzed by live-cell wide-field microscopy. Representative images of MMP2 trafficking after 0, 30, 35, and 40 min of biotin incubation. Images were acquired in 1-min frames for each analyzed cell. Arrowheads, cytoplasmic MMP2 vesicles. Scale bars, 10  $\mu$ m. (B) Quantification of cytoplasmic MMP2 vesicles per frame from cells shown in A. n.s., nonsignificant. \*,  $P < 0.05$ ; \*\*,  $P < 0.01$ . (C) Schematic representation of ER–Golgi cargo transport analysis, measured as normalized Golgi area over time in cells shown in A. (D) Normalized Golgi area for each time point (median  $\pm$  IQR). A reduced Golgi compaction was observed in the time range 15–23 min in NUCB1-KO cells compared with HeLa control. \*,  $P < 0.05$ . (E and F) HeLa or NUCB1-KO cells ( $n = 11$ ) expressing SS-SBP-MMP2-eGFP fixed without biotin addition and immunostained for ER exit site marker Sec16 (red). Scale bar, 10  $\mu$ m; zoom, 2  $\mu$ m. Retained MMP2 in the ER partially colocalized with Sec16 in both control and NUCB1-KO cells to the same extent (F). Magenta arrowheads, MMP2 structures that colocalized with ER exit sites; white arrowheads, ER exit sites.  $t$  test:  $P < 0.05$ .

NUCB1 MDA-MB-231-silenced cells. Upon collection of cell culture media and whole-cell lysate, WB analysis revealed reduced MMP2 secretion in NUCB1-silenced cells compared with control (Fig. 7, D and E), validating our findings with overexpressed MMP2-eGFP in HeLa cells (Fig. 2, E and F).

To assess the invasive phenotype of NUCB1 silencing in these cells, we performed Transwell invasion and gelatin degradation

assays. Compared with control cells, gelatin degradation in both NUCB1- and MMP2-silenced cells was significantly reduced; however, only NUCB1 depletion also had a significant impact on cell invasion (Fig. 7, F–I). These results illustrate the critical role played by NUCB1 in the trafficking of MMPs.

We next investigated whether the silencing of NUCB1 in human blood-derived primary macrophages (Fig. 8 A) would



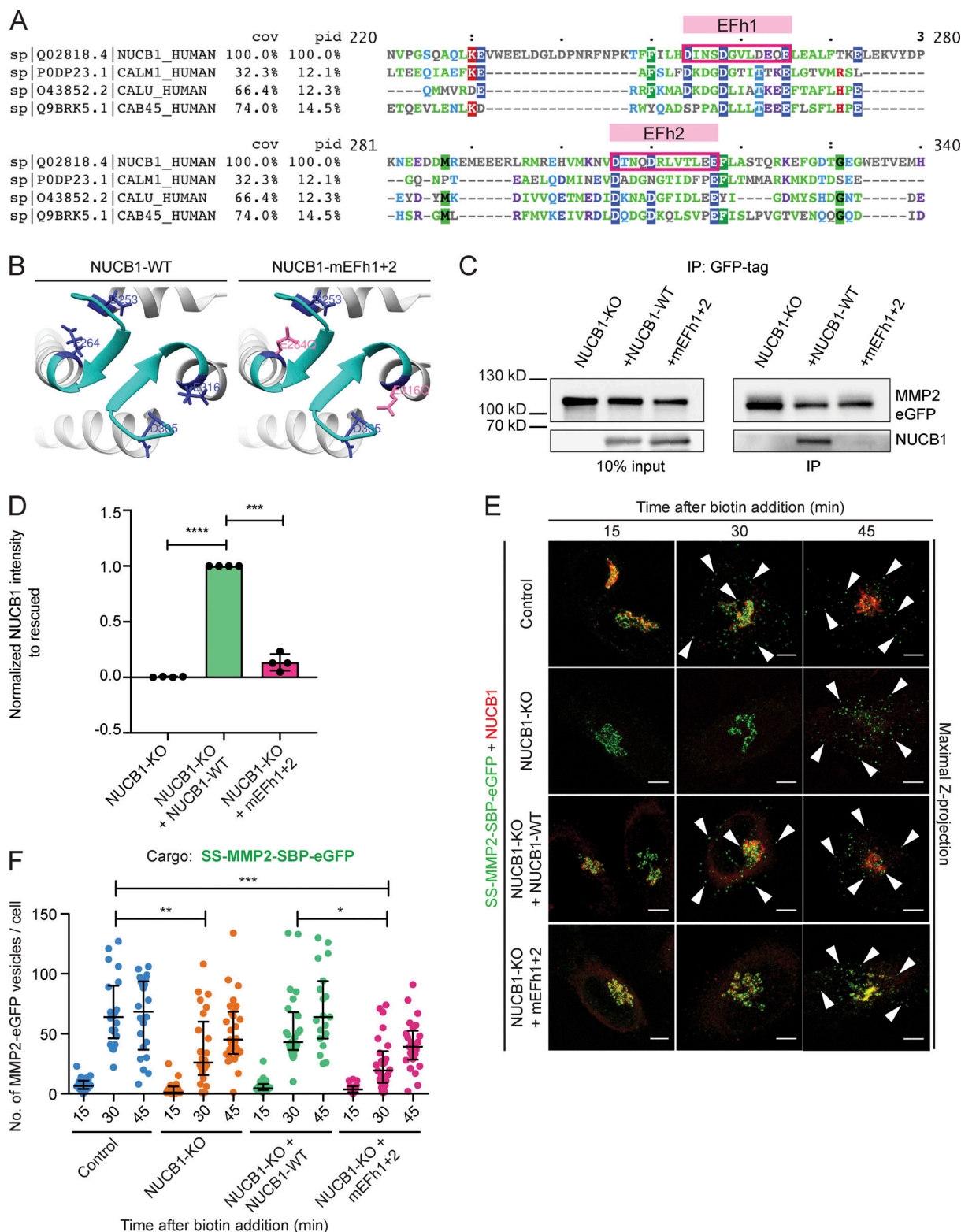


**Figure 5. NUCB1 EFhs are essential for Golgi trafficking of MMP2. (A)** Protein alignment of human NUCB1 (Q02818, aa 241–400), CaM (P0DP23), Calumenin (O43852), and Cab45 (Q9BRK5). Pink boxes, NUCB1 EFhs. **(B)** NUCB1 adapted PDB protein model (accession no. 1SNL); NUCB1 EFhs, cyan; NUCB1-WT, EFhs with first and last amino acid of the domain in dark blue; NUCB1-mEFh1+2, amino acid substitutions E264Q and E316Q in pink. **(C)** CoIP of MMP2-eGFP transiently expressed in NUCB1-KO cells transfected with NUCB1-WT or NUCB1-mEFh1+2.  $n = 4$  biological replicates. **(D)** Semiquantitative analysis of NUCB1 signal per sample normalized to the one of NUCB1-KO cells reexpressing NUCB1-WT. Bars, mean  $\pm$  SD; one-sample t test. **(E)** Confocal fluorescence images of HeLa or NUCB1-KO cells expressing SS-MMP2-SBP-eGFP and cotransfected with or without NUCB1-WT or NUCB1-mEFh1+2. After 15, 30, and 45 min of biotin incubation, cells were fixed and costained with NUCB1 antibody (red). Scale bars, 5  $\mu$ m. Arrowheads, cytoplasmic vesicles. **(F)** Quantification of cytoplasmic vesicles as in E from two independent experiments (median  $\pm$  IQR,  $n \geq 19$  cells). \*,  $P < 0.05$ ; \*\*,  $P < 0.01$ ; \*\*\*,  $P < 0.001$ ; \*\*\*\*,  $P < 0.0001$ .

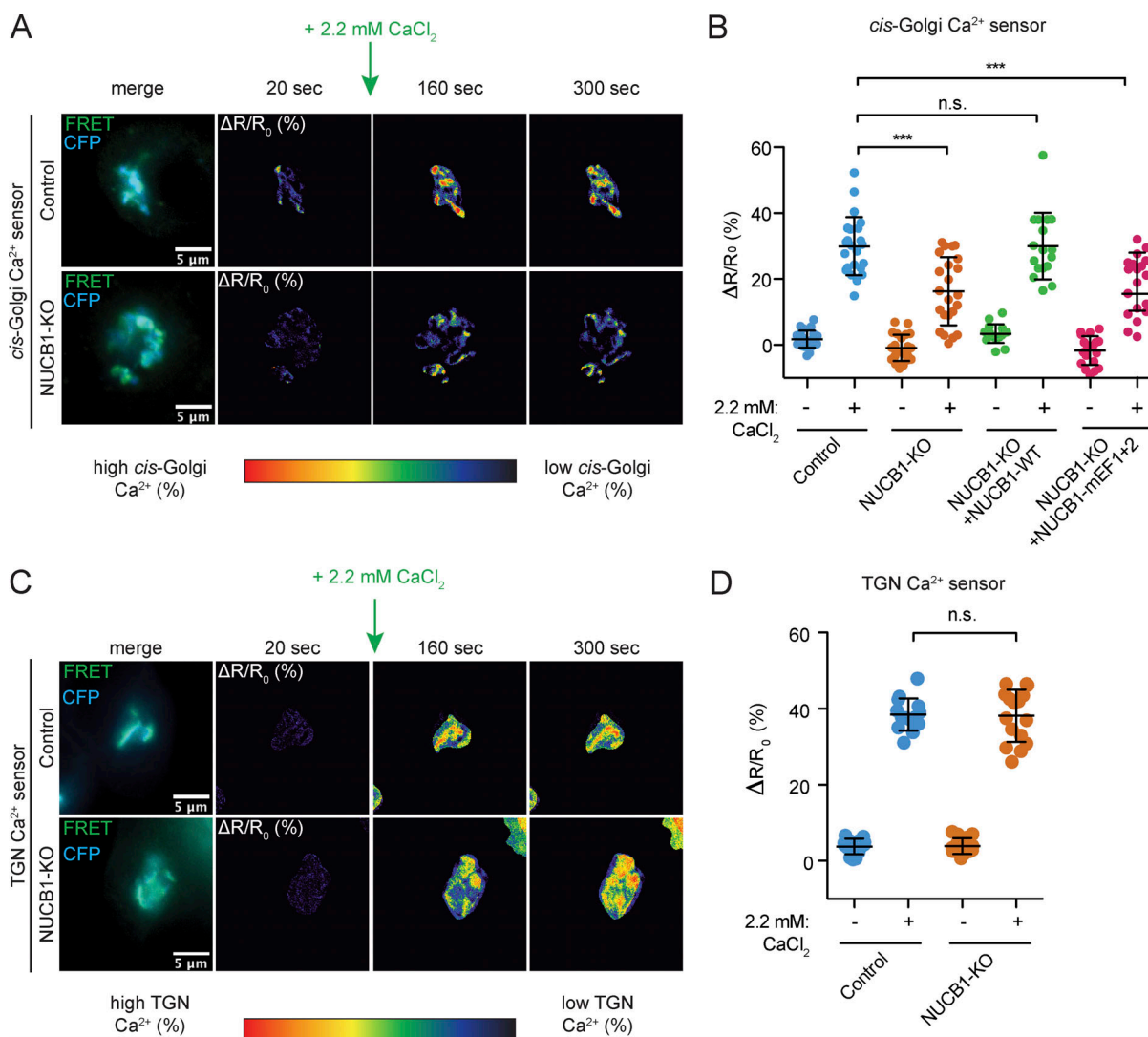


**Figure 6. NUCB1 EFhs are essential for  $\text{Ca}^{2+}$  homeostasis at the cis-Golgi.** (A) Fluorescent images of HeLa or NUCB1-KO cells expressing the GPP130-Twitch5 cis-Golgi  $\text{Ca}^{2+}$  sensor. Cells were treated with ionomycin for 20 s to deplete endogenous  $\text{Ca}^{2+}$  in the Golgi lumen; 2.2 mM  $\text{Ca}^{2+}$  were added, and cells were monitored using life-cell ratiometric FRET microscopy. (B) Quantification of the cis-Golgi  $\Delta R/R_0$  FRET ratio from A. (C) Pictures illustrate the same experiment described in A but using the Go-D1-cpv trans-Golgi  $\text{Ca}^{2+}$  sensor. (D) Quantification of the trans-Golgi  $\Delta R/R_0$  FRET ratio from C. Quantification of  $\geq 20$  cells (median  $\pm$  IQR) from at least two independent experiments. n.s., not significant; \*\*\*,  $P < 0.001$ .

also display a similar phenotype. To this end, human primary macrophages were seeded onto Rhodamine-labeled gelatin, incubated for 6 h, and evaluated by confocal microscopy. The degree of gelatin degradation was estimated as the Rhodamine intensity under each cell normalized by the intensity of the surrounding area and compared with the silenced control cells (siControl -LUC-). Interestingly, we observed a significant reduction in the number of degraded spots of both NUCB1- and MMP2-silenced cells compared with the control (Fig. 8, B and C), but no significant difference was observed between MMP2 and NUCB1 knockdowns.

Taken together, these results illustrate the striking effect of NUCB1 in MMP2 trafficking of human invasive cell models, both in human primary macrophages and under pathological conditions (as observed with MDA-MB-231 cells), and highlight the

importance of NUCB1 in the IG trafficking of MMPs and its impact on ECM remodeling.

## Discussion

MMPs are the central drivers for ECM turnover and invasive cell migration (Cauwe and Opdenakker, 2010; Shimoda and Khokha, 2017; Cui et al., 2017; Hannocks et al., 2019; Jobin et al., 2017). To date, known regulators of intracellular MMP transport include cytosolic factors such as microtubules that, in collaboration with motor proteins such as kinesins, steer TGN-derived vesicles toward the cell surface (Poincloux et al., 2009; Sbai et al., 2010; Wiesner et al., 2010; Cornfine et al., 2011; Gueye et al., 2011; Jacob et al., 2013). In addition, cytosolic Rab GTPases play an essential role in MMP trafficking and recycling (Bravo-Cordero et al., 2007; Jacob et al., 2013; Wiesner et al., 2013). Our colocalization

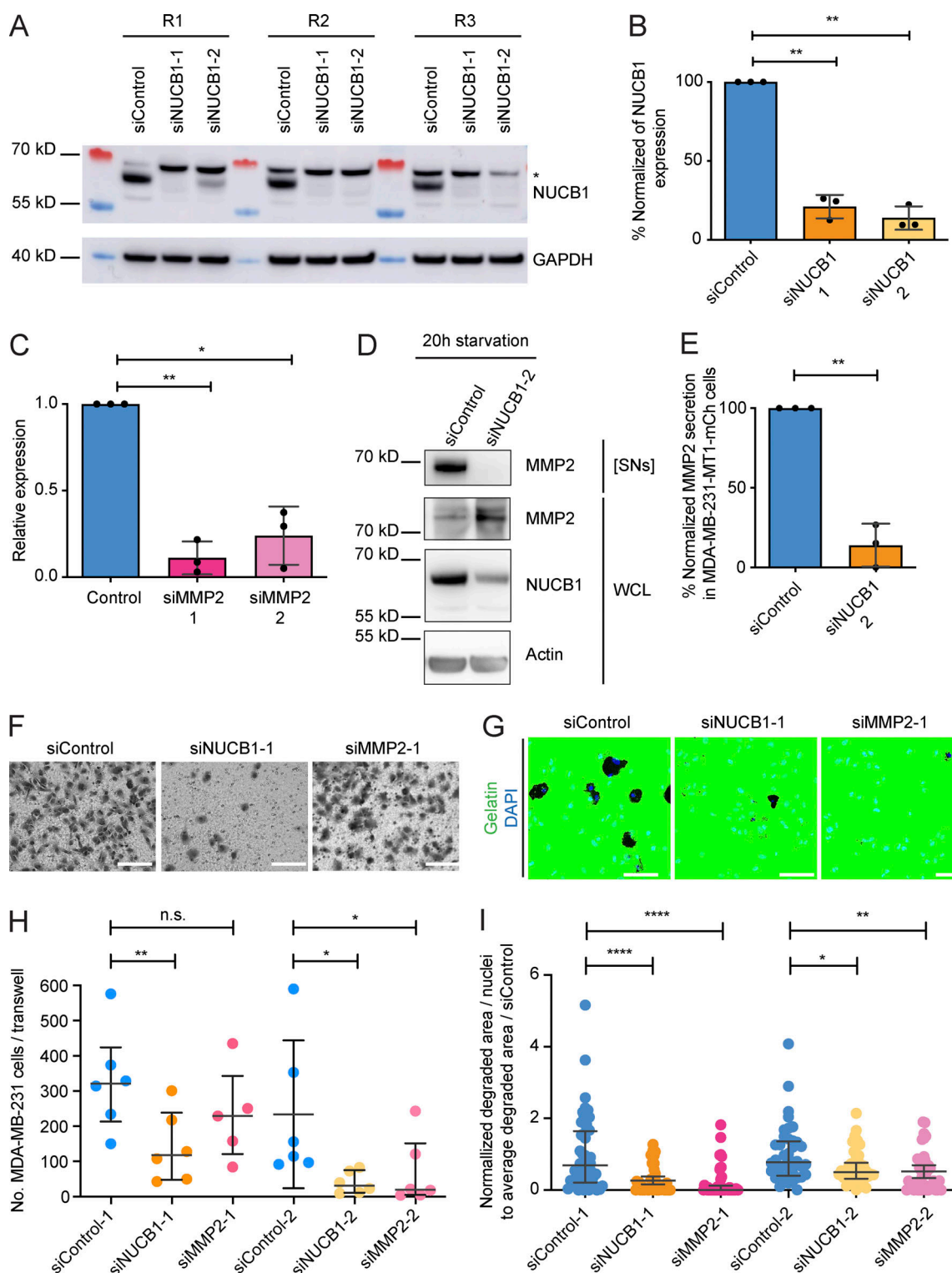


**Figure 7. NUCB1 depletion impairs ECM invasion and degradation in MDA-MB-231 cells.** (A) Expression levels of NUCB1 after siRNA-mediated silencing ( $n = 3$  independent experiments: R1, R2, and R3). \*, unspecific band. (B) Semiquantitative analysis of normalized NUCB1 signal from A in silenced cells compared with control. Bars, mean  $\pm$  SD. (C) Quantitative PCR analysis of relative MMP2 expression in siRNA-treated MDA-MB-231 cells ( $n = 3$  independent experiments, one-sample  $t$  test). (D) Secretion assay of endogenous MMP2 in MDA-MB-231 cells. [SN], 20 $\times$ -concentrated supernatant; WCL, whole cell lysates. (E) Semiquantitative analysis of three independent experiments. Bars, mean  $\pm$  SD. Significance, one-sample  $t$  test. (F and G) Representative pictures of Matrigel-coated Transwell invasion (F) or gelatin degradation (G) experiments. Scale bars, 150  $\mu$ m. (H and I) Quantification of the number of migrating cells (H) and degraded gelatin area (I). Both invasion and degradation were reduced in siNUCB1 cells. Data: median  $\pm$  IQR;  $n = 3$  independent experiments. Paired  $t$  test: \*,  $P < 0.05$ ; \*\*,  $P < 0.01$ ; n.s., not significant.



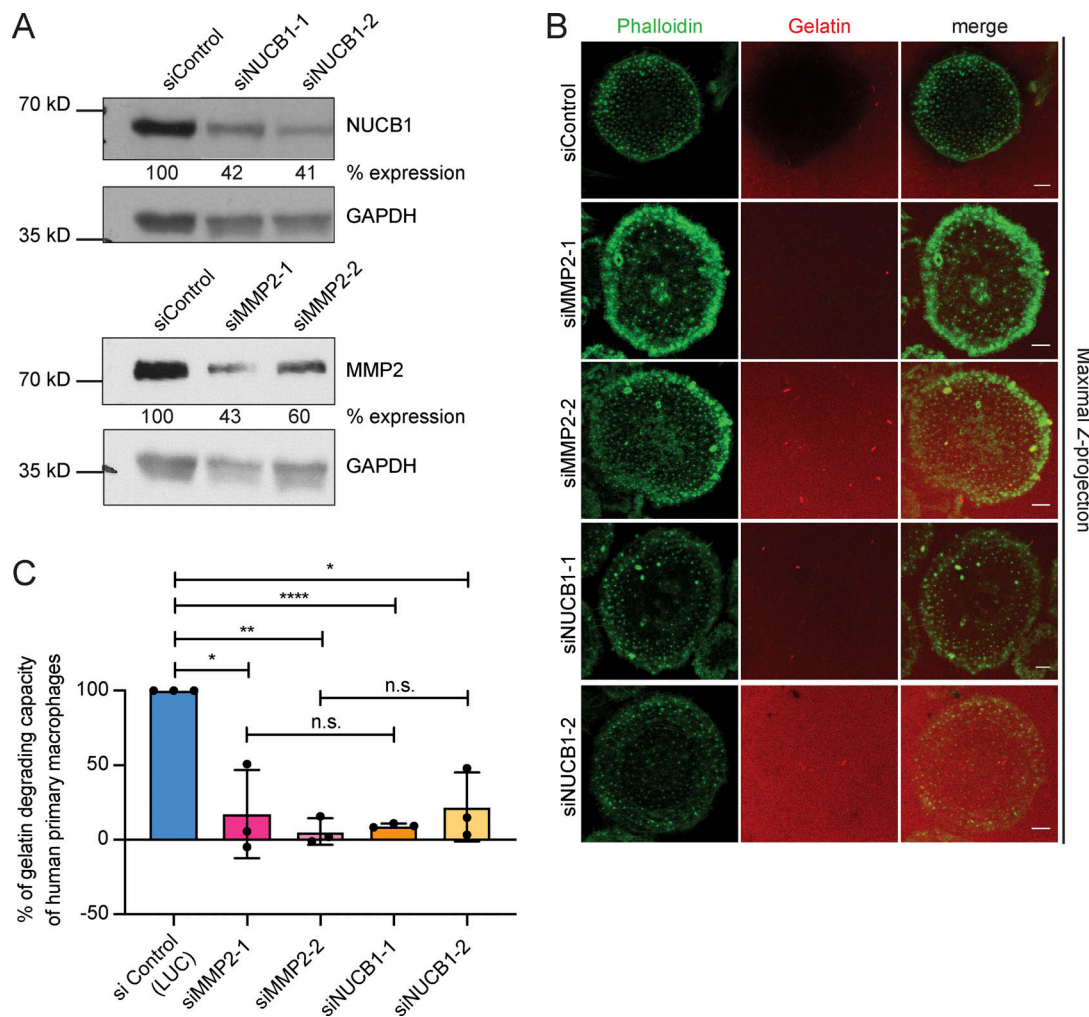


**Figure 8. Matrix degradation is reduced in NUCB1-silenced human primary macrophages.** (A) Validation of NUCB1 silencing. WB is representative of at least three independent experiments. %, relative expression compared with siControl. (B) Representative images of human-derived primary macrophages seeded on Rhodamine-conjugated gelatin and incubated for 6 h. Scale bars, 5  $\mu$ m.  $n = 3$  donors. (C) Quantification of gelatin degrading capacity of human primary macrophages. Bars, % of degraded gelatin compared with siControl. At least eight fields of view per condition were analyzed. Data: median  $\pm$  IQR. One-sample  $t$  test: \*,  $P < 0.05$ ; \*\*,  $P < 0.01$ ; \*\*\*,  $P < 0.001$ ; \*\*\*\*,  $P < 0.0001$ ; n.s., not significant.

experiments using different Rab proteins and MMP2-eGFP (Fig. S2) showed no colocalization with classic markers for TGN-derived vesicles such as Rab8 and Rab6. Also, we did not observe colocalization between MMP2-eGFP vesicles and early endosomes (Rab5), late endosomes (Rab7), recycling endosomes (Rab11), or lysosomes (mCherry-lysosomes), although a partial overlap was observed with LyzC in TGN-derived vesicles, suggesting a possible shared carrier for MMP2 and LyzC transport from the TGN to the plasma membrane.

Molecular mechanisms of anterograde cargo transport through the Golgi remain a major question in the field of membrane trafficking (Malhotra et al., 1989; Glick and Malhotra, 1998; Glick and Luini, 2011; Beznoussenko et al., 2014; Mironov and Beznoussenko, 2019). In this context, there is still a big debate in the field about how anterograde cargo, such as MMPs that arrive in the cis-Golgi, are segregated from retrograde cargo trafficking to the ER (Glick and Nakano, 2009; Mironov and Beznoussenko, 2019; Kurokawa et al., 2019).

To gain insight into this process, we combined a RUSH trafficking assay with MS to identify IG MMP2 interactors. This approach revealed NUCB1 as an interactor of MMP2, and this interaction seems to be direct, as we can detect the complex in solution by AUC (Fig. S3, D and E). Furthermore, the number of MMP2 and MT1-MMP secretory vesicles was significantly reduced in NUCB1-KO cells after 30 and 60 min of release, respectively, demonstrating that NUCB1 modulates their transport in living cells.

At which step of the secretory pathway, then, is MMP2 trafficking impaired? Colocalization experiments using ER-GIC53, GM130, and TGN46, as well as live-cell microscopy experiments, showed a delay in the cis-Golgi, where NUCB1 localizes. In contrast, ER export and TGN-to-cell surface targeting of MMP2 seem to be intact.

It remains unclear, though, why a delay rather than a complete block of trafficking occurs at the cis-Golgi. We speculate that there are compensatory mechanisms present in the Golgi:

for instance, several EFh  $\text{Ca}^{2+}$ -binding proteins in the Golgi may have similar functions (Honore, 2009). For example, calumenin is broadly distributed throughout the secretory pathway, but its function is not well understood (Vorum et al., 1999). Nevertheless, it has been demonstrated that it interacts with ECM proteins in the Golgi, such as thrombospondins (Hansen et al., 2009), and could play a role in their transport through the secretory pathway. Moreover, EFh proteins, such as calumenin and Cab45, travel through the cis-Golgi compartment and might partially compensate for the loss of NUCB1. In this scenario, a full compensation would not be possible because these proteins are not concentrated in the cis-Golgi.

### Luminal $\text{Ca}^{2+}$ in the Golgi evolves as an overall regulator of protein transport

Previous work has shown that  $\text{Ca}^{2+}$  channels and  $\text{Ca}^{2+}$  pumps, as well as  $\text{Ca}^{2+}$ -binding proteins, generate and maintain a concentration gradient inside the Golgi stack, with cis-Golgi containing the highest  $\text{Ca}^{2+}$  concentration (Missiaen et al., 2004; Vanoevelen et al., 2004, 2005; Lissandron et al., 2010; Pizzo et al., 2010; Aulestia et al., 2015). NUCB1 localizes to the cis-Golgi and has been proposed to regulate  $\text{Ca}^{2+}$  homeostasis in the lumen of this compartment (Lin et al., 1998, 1999; de Alba and Tjandra, 2004; Kanuru et al., 2009). Interestingly, we observed that NUCB1 absence affects  $\text{Ca}^{2+}$  homeostasis of the cis- but not trans-Golgi compartment, suggesting that these compartments are separate entities with individual regulation of their luminal  $\text{Ca}^{2+}$  content. Because NUCB1-KO induces a loss in luminal cis-Golgi  $\text{Ca}^{2+}$ , it might be also a regulator of SERCA pumps, as suggested by Lin et al. (1999).

What, then, is the role of luminal  $\text{Ca}^{2+}$  in the regulation of NUCB1 function? We evaluated the effect of  $\text{Ca}^{2+}$  in NUCB1 secondary structure via circular dichroism (CD) measurements. Using rNUCB1-His (Fig. S3 A) or recombinant NUCB1 with mutated EFhs (rNUCB1-mEFh1+2; Fig. S3, F and G), we observed a decreased molar ellipticity for rNUCB1-mEFh1+2 compared with rNUCB1-His (Fig. S3 H). These findings confirm that the NUCB1 EFh motifs have an open conformation under physiological conditions and fold upon  $\text{Ca}^{2+}$  addition, as described by de Alba and Tjandra (2004).

Interestingly, NUCB1 and Cab45 share similar features, such as the luminal exposure of their  $\text{Ca}^{2+}$  binding EFhs (Scherer et al., 1996; von Blume et al., 2012). Moreover, CD measurements of EFh pair domain mutants of His-SUMO-Cab45 showed a similar spectrum to the one observed in rNUCB1-mEFh1+2 (Crevenna et al., 2016; Deng et al., 2016). Furthermore, previous studies have shown that a local increase in  $\text{Ca}^{2+}$  provided by SPCA1 at specific TGN subdomains induces Cab45 oligomerization and sorting of soluble cargo molecules before their packing into sphingolipid-rich transport vesicles (Deng et al., 2018; Crevenna et al., 2016; von Blume et al., 2012). Finally, coIP experiments using NUCB1-mEFh1+2 clearly show that the interaction with MMP2 requires  $\text{Ca}^{2+}$  to promote its anterograde transport through the Golgi and final delivery at the cell surface. Taken together, these data propose that  $\text{Ca}^{2+}$  impacts several steps in IG transport and suggest that  $\text{Ca}^{2+}$  controls trafficking at sequential steps of cargo transport across a Golgi stack: NUCB1 at cis-Golgi and Cab45 at the TGN.

### Physiological role of NUCB1–MMP interaction

It is well known that both podosomes and invadopodia are cytoskeleton structures with a high proteolytic activity, which is needed for the proper invasion of interstitial tissue (Murphy and Courtneidge, 2011; Linder and Wiesner, 2016). In this regard, several studies have reported that MT1-MMP is a potential regulator of tumor invasion directly at the invadopodia mediating MMP secretion, activation, cell adhesion, and angiogenesis (Frittoli et al., 2011; Monteiro et al., 2013; Kajiho et al., 2016). In addition, MT1-MMP is the main source of MMP2 activation at the plasma membrane (Shaverdashvili et al., 2014; Han et al., 2015), both in steady state (Itoh, 2015; Sbaji et al., 2008) and under pathological conditions (Jacob et al., 2013, 2016), implying that an impairment or delay in its delivery can strongly inhibit cell invasion and ECM degradation.

In line with these data, we were able to show that NUCB1 is required for efficient trafficking of MT1-MMP through the Golgi, strongly supporting the role of NUCB1 as a critical component of MMP trafficking in the secretory pathway. Although the phenotype observed in matrix degradation of MMP2 in MDA-MB-231 siRNA-treated cells was expected, as gelatin is the principal substrate for MMP2 proteolysis, the impact on invasion in NUCB1-silenced cells is noticeable and hints toward a global modulation of MMP trafficking by NUCB1, which does not seem to be limited to the regulation of MMP2.

Based on the obtained data, we hypothesize that cis-Golgi-localized NUCB1 binds and concentrates incoming MMP2, and probably other MMPs such as MT1-MMP, at specific cis-Golgi “exit sites” at the rim of cisternae, where the vesicle transport machinery is known to accumulate (Farquhar, 1985; Orci et al., 1986; Lavieu et al., 2013; Dancourt et al., 2016; Dunlop et al., 2017; Ernst et al., 2018). EM studies have shown that cargo accumulates at these rims compared with the flatter center of the cisternae (Orci et al., 1986; Lavieu et al., 2013). Moreover, a recent paper by Ernst et al. (2018) uncovered a cargo sorting mechanism regulated by S-palmitoylation in the cis-Golgi that supports these findings. In this model, palmitoylation acts as a biophysical switch to sort cargoes to the cisternal rim of the Golgi, promoting their further transport (Ernst et al., 2018).

Furthermore, Lin et al. (1998) showed that, in contrast to Cab45, NUCB1 is bound to the luminal surface of Golgi membranes by an unknown mechanism. Based on these findings, we speculate that NUCB1 might interact with an unknown transmembrane protein anchored in the cis-Golgi membrane via palmitoylation. In this context, it is interesting to note that MT1-MMP is palmitoylated at Cys574 in its cytosolic domain (Anilkumar et al., 2005). Altogether, this evidence suggests that NUCB1 could be enriched at palmitoylated cis-Golgi rims, which allow MMP molecules to concentrate in a  $\text{Ca}^{2+}$ -dependent manner to facilitate vesicle or tubule budding from the cisternal rim by local membrane bending.

Another possibility is that NUCB1 associates to the membrane in a  $\text{Ca}^{2+}$ -dependent manner or via conformational changes after cargo binding. In this regard, our CD measurements showed that NUCB1 acquires a compact conformation upon  $\text{Ca}^{2+}$  addition, and this change may expose residues that have a higher affinity for negative charges, stimulating NUCB1 association with

cis-Golgi membranes. We speculate that this association could stochastically accumulate MMP cargo and facilitate MMP trafficking to the next compartment in a protein maturation-dependent manner. This hypothesis would be in line with previously published *in vitro* data that postulate NUCB1 as a chaperone-like protein (Bonito-Oliva et al., 2017; Kanuru and Aradhyam, 2017).

Whether NUCB1 acts as a “switch protein” or exerts a chaperone-like activity on MMP2 at the cis-Golgi remains to be elucidated in future studies. The role of NUCB1 on the proper maturation of MMPs should be addressed to elucidate a more comprehensive mechanism of MMP trafficking. Further investigation is required to determine which other components might influence MMP sorting, as well as how impaired  $\text{Ca}^{2+}$  homeostasis by NUCB1 depletion delays cargo trafficking.

In conclusion, we report for the first time the involvement of NUCB1 and  $\text{Ca}^{2+}$  in MMP2 IG trafficking. This process promotes MMP2 anterograde transport along the secretory pathway and is essential for efficient ECM remodeling in both breast cancer cell lines and primary human macrophages. Our findings encourage the exploration of regulators of MMP trafficking as alternative targets to therapeutically modulate cell invasion.

## Materials and methods

### Cell culture

HeLa cells were obtained from Cell Line Service, and HEK293T cells from the American Type Culture Collection (ATCC; CRL-3216). Regular evaluation for mycoplasma contamination was performed to guarantee mycoplasma-free cell culture (LookOUT, MP0035; Sigma-Aldrich). These cell lines were cultured in DMEM supplemented with 10% FCS and 1% penicillin/streptomycin at 37°C and 5%  $\text{CO}_2$ . To generate the CRISPR/Cas9 KO cell lines, viral infection was performed using a method described by Crevenna et al. (2016).

For recombinant protein production, stable cell lines were generated using the piggyback system in HEK293T cells. rHS-MMP2, rNUCB1-His, and rNUCB1-mEFh1+2 pB-T-PAF constructs were transfected together with pBase and pB-RN constructs using linear polyethyleneimine (PEI; Alfa Aesar Chemicals) and 1.5  $\mu\text{g}$  of DNA. After overnight incubation, the medium was replaced, and cells were allowed to recover for 24 h. The cells were selected with puromycin (1  $\mu\text{g}/\text{ml}$ ) and G418 (0.5  $\mu\text{g}/\text{ml}$ ) for at least 24 h. The medium was replaced, and cells were allowed to recover and expand. Confirmation of the stable cell line was performed via WB analysis.

MDA-MB-231 cells stably expressing mCherry-MT1-MMP (kindly provided by Philippe Chavrier, Institut Curie, Paris, France) were cultured in Leibovitz L-15 medium (Thermo Fisher Scientific) supplemented with 15% FCS and 50 ng/ml G418 (Calbiochem) in a humidified atmosphere with 1%  $\text{CO}_2$  at 37°C. All cell lines tested negative for mycoplasma (LT07-318, Mycoplasma Detection Kit; Lonza) and were maintained in culture for  $\leq 3$  mo.

### Isolation and culture of primary human macrophages

Human peripheral blood monocytes were isolated from buffy coats as described previously (Wiesner et al., 2013). The analysis

of anonymized blood donations was approved by the Ethical Committee of the Ärztekammer Hamburg (Hamburg, Germany). Cells were cultured in RPMI 1640 (containing 100 units/ml penicillin, 100  $\mu\text{g}/\text{ml}$  streptomycin, 2 mM glutamine, and 20% autologous serum) at 37°C, 5%  $\text{CO}_2$ , and 90% humidity. Monocytes were differentiated in culture for  $\geq 7$  d with the addition of 20% human autologous serum.

### Antibodies

MMP-2 and Rab11 antibodies were purchased from Abcam (rabbit ab92536 and rabbit ab3612, respectively). NUCB1,  $\beta$ -actin, and monoclonal anti-FLAG M2 peroxidase antibodies were obtained from Sigma-Aldrich (rabbit HPA008176 and mouse A5441 and A8592, respectively); ERGIC53 was acquired from ENZO Life Sciences (mouse ENZ-ABS300); GM130 antibody and  $\beta$ -integrin were purchased from BD Bioscience (mouse 610822 and mouse 610467, respectively); Rab5, Rab7, and streptavidin-HRP antibodies were from Cell Signaling (rabbit C8B1, D95F2, and 3999S, respectively); and TGN46 antibody was obtained from AbD Serotec (sheep AHP500G). MMP-14 antibody was purchased from Millipore (mouse MAB3328), and GFP antibody (rabbit sc8334) and HRP-coupled secondary antibodies (anti-rabbit IgG, anti-mouse IgG, and anti-sheep IgG) were purchased from Santa Cruz Biotechnology. Sec16A antibody (KIAA0310 polyclonal rabbit) was purchased from Biomol (now Thermo Fisher Scientific, A300-648A-M). Anti-rabbit HRP antibody used with primary macrophages was purchased from Cell Signaling (7074). The Alexa Fluor secondary antibodies used for immunofluorescence (488, 594, 633, and phalloidin-Alexa Fluor 488, different species) were purchased from Thermo Fisher Scientific.

### Other reagents

All cell culture reagents (DMEM medium + glucose, FCS, and penicillin/streptomycin) were obtained from Gibco-Thermo Fisher Scientific. The SDS gels used for MS were purchased from Invitrogen (NP0321BOX, NuPAGE 4–12% Bis-Tris Protein Gels, 1.0 mm, 10-well). All restriction enzymes were purchased from New England Biolabs. cOmplete Tablets, Mini EDTA-free, EASYpack protease inhibitor tablets (from here on, cOmplete tablets) were purchased from Roche Diagnostics.

### Plasmids

The human *MMP2* gene was amplified from a pCMV3-SP-Flag-MMP2 vector (Sino Biological) using 5'-CCCAAGCTTATGCCA CTGCTGCTCTTGCT-3' as a forward (Fw) primer and 5'-TTTTCCTTTTGCGGCCGCTCAAGCGTAATCTGGAACATCGTATGGGTA GCAGCCTAGCCAGTCGGATTT-3' as a reverse (Rv) primer. For the RUSH experiments, the gene was engineered by substitution of ST in a Str-KDEL-ST-SBP-EGFP vector (Addgene\_65264), using the following pairs of primers: (a) Fw: 5'-TTGGCGGCCAT GGCTACAGGCTCCCGAC-3', Rv: 5'-CTTATCGTCGTCATCCTT GTAATCGGATAAGGGAATGGTTGGGAAGGC-3'; and (b) Fw: 5'-GCCTTCCCAACCATTCCCTTATCCGATTACAAGGATGACGAC GATAAG-3', Rv: 5'-CCGGAATTCCCCAGCGTAATCTGGAACATC GTATG-3'. The fragment was inserted after the sequence of the signal peptide of human growth hormone, and all plasmids containing this as signal sequence are named SS-(construct).



For the CRISPR-KO of NUCB1, we used a pSpCas9(BB)-T2A-Puro (PX459) backbone vector (Addgene\_48139) containing the following guide RNA: 5'-CACGGCTCCTGCTTCGCGCCGTGC-3', which was designed using the Optimized CRISPR design tool from Zhang Lab (<https://zlab.bio/guide-design-resources>, accessed on August 7, 2017).

The SS-Flag-MMP2-HA-eGFP construct was cloned using Gibson assembly with two fragment insertion and the following primers: Fw1: 5'-GGGCCCCATAAAGCTTATACGAATTCATGGCTACAGGCTCCCGGAC-3', Rv1: 5'-TCCTCGCCTTTGCTCACCATA GCGTAATCTGGAACATCGTATGGTA-3'; and Fw2: 5'-TACCCA TACGATGTTCCAGATTACGCTATGGTGAGCAAAGGCGAGGA-3', Rv2: 5'-GCGGCCGCTTGTGCGACACTCGAGTTAAGGCCGGCCCTT GTACAG-3'. For this cloning, the restriction enzymes EcoRI and XhoI were used. The SS-LyzC-SBP-eGFP construct was previously reported by Deng et al. (2018).

For the rescue experiments, we performed Gibson assembly to insert the NUCB1 gene myc tagged from a pCMV3 vector from OriGene (RG201786) in a pLPCX vector using HindIII-HF and BamHI. The Fw primer was 5'-GATCTGGGCCCCATAAAGCTTC CATGCCTCCCTCTGGGC-3', and the Rv primer was 5'-CGACAC TCGAGTATGGATCCTCACAAGTCTTCTTCAGAGATGAGTTTC TGCTCCAGATGCTGGGGCACCTCAAC-3'. To generate the EFh-binding mutants of NUCB1, we substituted E264Q and E316Q via Gibson assembly using two complementary fragments amplified with the primers Fw1: 5'-CGGACTCAGATCTGGGCCATAAA GCTTCCATGCCTCCCTCTGG-3'; Fw2: 5'-GGATGAGCAGCAGCT GGAGGCAC-3'; Rv1: 5'-GTGCCTCAGCTGCTGCTCATCC-3'; and Rv2: 5'-CCCTTTTTCTGGAGACTAAATAAAATCTTTTATTTTA TCGATGTATATGCTCACAAGTCTTCTTCAGAGATGAGTTTCTG CTCC-3'. The nontagged version of NUCB1-WT was inserted in the pLPCX backbone by restriction cloning of the pCMV3 vector from OriGene (see above) using EcoRI and NotI. The GFP-HA plasmid used as a control contained the acGFP sequence C-terminally tagged with HA in a pLPCX vector.

For the expression of a HIS-SUMO-tagged version of MMP2 in HEK293T cells, cDNA was amplified from the pLPCX-SS-Flag-MMP2-HA-eGFP plasmid using the primer pair 5'-GGCGGCCAT CACAAGTTTGTACAGCTAGCATGGCTACAGGCTCCCGGAC-3' (Fw) and 5'-GGCGGCCATCACAAGTTTGTACAGCTAGCATGG CTACAGGCTCCCGGAC-3' (Rv). A GST tag also was amplified using the primer pair 5'-CAAATCCGACTGGCTAGGCTGCATGTC CCCTATACTAGGTTATTG-3' and 5'-CCAGCACACTGGATCAGT TATCTATGCGGCCGCTTAGATCCGATTTTGGAGGATGGTC-3'. Together, the fragments were inserted into a pB-T-PAF Vector (Core Facility, Max Planck Institute of Biochemistry) using Gibson assembly to generate a plasmid coding for MMP2-GST fusion protein, which was then used as a template to amplify the MMP2 sequence with the plasmids 5'-GAACAGATTGGAGGT GAATGCGATTACAAGGATGACGACGATAAG-3' (Fw) and 5'-GATCAGTTATCTATGCGGCCGCTCAGCAGCCTAGCCAGTCGG ATTTG-3'. The His-SUMO sequence was amplified from a vector published by Crevenna et al. (2016), and both fragments replaced the Cab45 cassette in the mentioned plasmid using Gibson assembly.

For the expression of the His-tagged version of NUCB1-WT (rNUCB1-His), cDNA sequence was amplified from the pLPCX-

NUCB1-myc construct using the primer pair 5'-GGCGGCCAT CACAAGTTTGTACAGCTAGCCATGCCTCCCTCTGGGC-3' (Fw) and 5'-GCGGCCGCTTGTGCTAGTGATGATGATGGTGATGACCGCT CCACCCAGATGCTGGGGCACCTCAAC-3' (Rv) and inserted in the pB-T-PAF backbone using NheI and NotI restriction enzymes. For the expression of the His-tagged version of NUCB1-EFh1+2 (rNUCB1-mEFh1+2), cDNA sequence was amplified from the pLPCX-NUCB1-EFh1+2 construct using the primer pair 5'-GGCGGCCATCACAAGTTTGTACAGCTAGCCATGCCTCCCTCT GGG-3' (Fw) and 5'-GCGGCCGCTTGTGCTAGTGATGATGATGGTGA TGACCGCTCCACCCAGATGCTGGGGCACCTCAAC-3' (Rv). All primers were purchased from Metabion International.

The Twitch 5 Ca<sup>2+</sup> sensor was kindly provided by Oliver Griesbeck (Max Planck Institute of Neurobiology, Martinsried, Germany; Thestrup et al., 2014). The plasmid carrying rat-GP130 cis-Golgi targeting sequence pME-zeo-GP130-pHluorin was kindly provided by Yusuke Maeda (Research Institute for Microbial Diseases, Osaka, Japan; Maeda and Kinoshita, 2010). The Twitch 5 ORF was amplified using primers Twitch5-MluI forward, 5'-CACACGCGTGTGAGCAAGGGCGAGGAG-3', and reverse, 5'-CACGCGGCCGCTCAATCCTCAATGTTGTGACGG-3', and inserted into pME-zeo-GP130-pHluorin using MluI and NotI restriction enzymes and replacing the pHluorin fragment.

The luminal part of human MT1-MMP (MMP14, NP\_004986.1) was amplified via PCR using the primer pair 5'-AAG TGGCGCGCCATGTCTCCCGCCCCAAGA-3' and 5'-GCGCGAATT CGCTCCGCCCTCTCGTCCA-3' from a plasmid containing MT1-MMP-mCherry (kind gift of P. Chavrier, Institut Curie, Paris, France). This fragment was then inserted into the RUSH plasmid Str-KDEL\_SS-SBP-EGFP (Boncompain et al., 2012) using AscI and EcoRI restriction enzymes. The fragment coding for the transmembrane and cytoplasmic domains of MT1-MMP was amplified by PCR using the primer pair 5'-AGATGGCCGGCCATT AGGCGGGGCGGTGAGCG-3' and 5'-AATCGGCCCTCGAGGCCCT CAGACCTTGTCAGCAGGG-3'. The PCR fragment was then inserted into the previously described plasmid using FseI and SfiI restriction enzymes. This cloning strategy generated a plasmid coding for Str-KDEL\_MT1-MMP-SBP-EGFP with SBP-EGFP cassette located between the luminal and transmembrane domains of MT1-MMP. The EGFP cassette was then replaced by an mCherry coding sequence obtained from the RUSH plasmid Str-KDEL\_SBP-mCherry-GPI using BsrGI and SbfI restriction enzymes. The mCherry-Lysosome construct was a gift from Florian Basserman (Technische Universität, München, Germany). Rab6-GFP and Rab8-GFP constructs were a gift from Vivek Malhotra (Centre for Genomic Regulation, Barcelona, Spain).

### Oligonucleotides

siRNAs were purchased from Life Technologies, with the following epitopes: 5'-UCAUGCAGUAUGAAGAAGGUCUUGG-3' (siN UCB1-1), 5'-GAGCUGGAGAAAGUGUACGACCCAA-3' (siNUB1-2), 5'-AGUAGAUCAGUAUUCUACUCCUGC-3' (siMMP2-1), and 5'-CCAGAUGUGGCCAACUACAACUUCU-3' (siMMP2-2).

### siRNA treatment

MDA-MB-231 cells were transfected with a negative siRNA control (4390843; Life Technologies) and with NUCB1 or MMP2

siRNA at a final concentration of 5 nM using RNAiMax (Life Technologies) according to the manufacturer's instructions. siRNA targeting firefly luciferase mRNA (D-001210-02-20; Dharmacon) was used as a negative control in primary human macrophages, which were transfected with NUCB1 or MMP2 siRNA at a final concentration of 100 nM. Knockdowns were achieved 72 h after transfection using the Viromer Blue Kit according to the manufacturer's instructions. Reduction of targeted proteins was validated by WB of respective cell lysates.

### Quantitative RT-PCR experiments

Total RNA was isolated from cells using the NucleoSpin RNA kit (Macherey-Nagel) according to the manufacturer's instructions. 100 ng of RNA was used for the real-time PCR reaction using the QuantiTect SYBR Green RT-PCR Kit (Qiagen). Quantitative RT-PCR was performed with a Cfx96 device (Bio-Rad) using a Power SYBR Green RNA-to-Ct 1-Step kit (Applied Biosystems). QuantiTect Primer assays (Qiagen) were used to amplify MMP2 (*Hs\_MMP2\_1\_SG*) and peptidylprolyl isomerase (*Hs\_PPIA\_4\_SG*), and changes in the relative expression levels were determined using the  $2^{-\Delta\Delta C_t}$  method (Bio-Rad CFX Manager software 3.1).

### IP

HEK293T or HeLa cells ( $3 \times 10^5$  cells/ml) were seeded in 15-cm plastic dishes (two per sample). After overnight incubation, each plate was transfected with 15  $\mu$ g DNA using 1.25 mg/ml PEI as a transfection reagent (DNA/PEI, 1:7.5) and incubated for 20 h. Cells were then washed twice with PBS, scraped, and centrifuged for 3 min at 3,400 rpm. Supernatants were discarded, and pellets were washed two more times. Then, 300  $\mu$ l lysis IP buffer (50 mM Tris, 150 mM NaCl, and 0.1% Triton X-100 + cOmplete tablets) were added, and samples were incubated for 30 min on ice. Samples were then filtered through a 27G needle and centrifuged at  $>13,000$  rpm, 4°C, for 5 min. Supernatants were placed in a new Eppendorf tube and centrifuged once more for  $\geq 20$  min,  $>13,000$  rpm, 4°C. Next, total protein was estimated using Bradford assay and normalized to the lowest protein concentration. A volume of 27  $\mu$ l per sample was taken, mixed with 9  $\mu$ l of 4 $\times$  Laemmli buffer and labeled as input sample (10% input). Then, 35  $\mu$ l of GFP beads, previously equilibrated with the lysis buffer, were added to the samples and incubated in an end-to-end rotator at 4°C for 1 h. Cells were centrifuged at 3,400 rpm, 4°C, for 3 min, supernatants were discarded, and samples were washed with 1 ml lysis buffer (1 $\times$  PBS + 1% Triton X-100). This step was repeated twice, and after the last removal of supernatant, 35  $\mu$ l Laemmli buffer 4 $\times$  was added to the samples, and the mixtures were incubated at 95°C for 10 min. Finally, the samples were centrifuged at maximal speed (room temperature), and supernatants were collected and labeled as IP sample for loading in 10% SDS gel.

For the IP experiments using rNUCB1-His,  $\sim 100$   $\mu$ l of the recombinant protein was dialyzed overnight using the Pur-A-Lyzer mini dialysis Kit (Sigma-Aldrich) in 500 ml of 50 mM Tris + 100 mM NaCl. After dialysis, protein concentration was determined via absorbance measurement at 280 nm using a Nanodrop ND-1000 Spectrophotometer (PEQLAB Biotechnology). Proteins were normalized and incubated with

previously washed Protino Ni-NTA agarose beads (Macherey-Nagel) for 2 h on a rotator at 4°C. At the same time, Golgi preps (prepared using a method described by von Blume et al. [2012]) were lysed using 50  $\mu$ l of the described lysis IP buffer for 15 min on ice and centrifuged at 13,200 rpm for 10 min to remove membranes. After incubation, beads were washed 5 $\times$  with lysis IP buffer and centrifuged at 3,400 rpm, 4°C, for 3 min each time. The lysed Golgi preps were added to the beads and incubated for 2 h with rotation at 4°C. After incubation, beads + Golgi preps were centrifuged at 3,400 rpm, 4°C, for 3 min. The beads were transferred to a new tube in the last step, 35  $\mu$ l of Laemmli buffer 4 $\times$  was added to the samples, and the mixtures were incubated at 95°C for 10 min. Finally, samples were centrifuged at maximal speed (room temperature), and supernatants were collected and labeled as IP sample for loading in a NuPAGE 4–12% Bis-Tris protein gel. The IP blot depicted (Fig. 1 G) is a mirrored image. Semiquantitative analyses of band intensities were performed using Fiji (ImageJ). Statistical evaluations are described in each figure legend.

### SDS-PAGE and WB

SDS-PAGE was performed using 10% homemade acrylamide gels or NuPAGE 4–12% gradient gels. For WB, samples were transferred to nitrocellulose membranes for 75 min and blocked in 5% BSA in Tris-buffered saline (TBS) for at least 1 h at room temperature. The membranes were incubated overnight with primary antibody in a shaker at 4°C, washed for 1 h with TBS + 0.1% Tween-20 (TBS-T), and incubated with secondary antibody for 2 h at 4°C. Then, membranes were washed for half an hour with TBS-T and documented in a ChemiDoc Imaging System (Bio-Rad), an ImageQuant LAS 4000 series (GE Healthcare Life Sciences), or an Amersham Imager 600 (GE Healthcare Life Sciences).

### MS analysis

MS samples were processed at the core facility of the Max Planck Institute of Biochemistry. Samples from gel lanes were digested with trypsin using in-gel digestion protocol, and peptides were extracted and purified via C18 StageTips. Peptides were analyzed in a Q Exactive HF machine with a data-dependent acquisition scheme using higher-energy collisional dissociation fragmentation. Raw data were processed using the MaxQuant computational platform, and the peak lists were searched against a human reference proteome database from Uniprot. All identifications were filtered at 1% false discovery rate and label-free quantitation. Proteomic data were analyzed with the Perseus 1.5.5.3 software (Tyanova et al., 2016), and results from a *t* test using Perseus were plotted as logarithmic ratios against logarithmic P values. The final selection of positive hits was done by filtering out potential contaminants, reverse sequences, and hits identified only by site.

### Immunofluorescence and confocal microscopy

HeLa cells ( $3 \times 10^4$  cells/ml) were seeded into six-well plates with two glass slides per well. After incubation for 24 h, the cells were transfected with PEI (2  $\mu$ g DNA, 15  $\mu$ l PEI, and 200  $\mu$ l OptiMEM) and incubated for no more than 24 h. Afterward, the

cells were washed three times with 1× PBS, fixed with 4% PFA for 10 min, and permeabilized with either 0.2% Triton X-100 and 0.5% SDS in PBS for 5 min or 0.05% saponin in 5% BSA in PBS for 1 h at room temperature (if no costaining was involved, cells were directly mounted after fixation). Subsequently, cells were incubated with 5% BSA in PBS overnight at 4°C. Primary antibody was added, and the mixture was incubated either overnight at 4°C or for 1 h at room temperature. After washing, secondary antibody was added and incubated for 1 h at room temperature. Finally, cells were mounted in glass slides using ProLong Gold antifade reagent (Invitrogen) and evaluated using confocal microscopy.

Images were acquired at 22°C on a Zeiss laser scanning LSM780 confocal microscope (Carl Zeiss) equipped with a 100× (NA 1.46, oil) objective. To detect Alexa Fluor, the 488-nm laser line was used. Pictures were acquired using Leica software (Zen 2010) and processed, merged, and gamma adjusted in ImageJ (v1.37).

Cellular vesicle number analysis was conducted using a custom-made ImageJ macro previously described (Deng et al., 2018). The macro uses ImageJ's rolling ball background subtraction algorithm, the "enhance contrast" function, and maximum z-projection of the RUSH reporter channel to cover all vesicles of the cell volume in a 2D image. After using a median filter, suitable cells were selected via polygon selection. A binary image was generated using the "threshold" function. The threshold algorithm "Yen" was used as default, whereas the threshold required manual correction for low-intensity images. The vesicle objects in the binary images were compared with the original image and controlled via visual inspection. In the binary image, vesicle objects with sizes 4–20 pixels were quantified using the Analyze Particles function. All macros used for image analysis are available at <https://github.com/MehrshadPakdel>.

### RUSH cargo sorting assay

The RUSH cargo sorting assay was performed as previously described (Deng et al., 2018). HeLa or NUCB1-KO cells were cultured on sterile glass slides in 6-well dishes. Cells were transfected using pIRESneo3-SS-Str-KDEL-Flag-MMP2-SBP-HA-eGFP, pIRESneo3-SS-Str-KDEL-acGFP-HA, pIRESneo3-Str-KDEL-LyzC-SBP-eGFP, pIRESneo3-SS-Str-KDEL-cathD-SBP-eGFP, or pIRESneo3-Str-KDEL-MT1MMP-SBP-mCherry alone or together with NUCB1-WT, NUCB1-WT-myc, or its EFh mutants for 16 h. Cells were incubated with 40 μM D-biotin (Supelco, 47868) in DMEM supplemented with 10% FCS and 1% penicillin/streptomycin for the indicated times. At time point 0, cells were incubated with complete medium without D-biotin to confirm reporter retention. The cells were then washed twice in 1× PBS, fixed in 4% PFA in PBS for 10 min, and further processed for immunofluorescence microscopy as described above. Samples were quantified using confocal microscopy. Only cells that showed proper reporter transport to the Golgi after biotin addition were processed, whereas those showing ER signal after biotin addition were discarded. To cover the whole volume of the cells, typically 8–16 z-stacks with a step size of 0.39 μm were acquired for each field of view.

### RUSH live-cell trafficking assay

We seeded 30,000 HeLa or NUCB1-KO cells into live-cell dishes (μ-Dish 35 mm, High Glass Bottom from Ibidi) and transfected

them the next day with the SS-SBP-MMP2-eGFP RUSH construct for 24 h. Cells were washed in PBS and incubated in DMEM, high glucose, Hepes, no phenol red (Gibco by Life Technologies). Image acquisition was performed at the Imaging Facility of the Max Planck Institute of Biochemistry on a GE DeltaVision Elite system based on an Olympus IX-71 inverted microscope, an Olympus 60×/1.42 PLAPON oil objective, and a PCO sCMOS 5.5 camera at intervals of 1 min per frame. At  $t = 0$  min of the video, DMEM + biotin was added to the cells to reach a final concentration of 40 μM biotin. Images were acquired using softWoRx 5.5 software (GE Healthcare).

### Live-cell vesicle image analysis

Quantification of cytoplasmic vesicles per frame was conducted using a custom-made ImageJ macro based on RUSH vesicle analysis, as described previously (Deng et al., 2018). The macro uses ImageJ's rolling ball background subtraction algorithm followed by a mean filter to smooth edges of the objects. A binary image was generated by the Auto Threshold function using the "minimum" algorithm for frames 1–25 and the "moments" algorithm for frames 26–45 to optimize image thresholding for ER-like objects and then for Golgi and vesicular structures. The vesicle objects in the binary images were compared with the original images and controlled via visual inspection. Finally, vesicle objects with sizes ranging between 4 and 40 pixels were quantified using the "analyze particles" function. Data from 17 HeLa and 22 NUCB1-KO cells from two independent experiments were plotted as the median ± IQR. Significant differences with  $P < 0.05$  were analyzed using the nonparametric Kruskal–Wallis test with Dunn's multiple comparison test.

### Live-cell ER–Golgi cargo transport analysis

Quantification of normalized Golgi area over time was conducted using the custom-made ImageJ macros. The first part of the macro used a median filter to smooth the edges of objects. A binary image was generated for the first frame of the video to extract the ER signal of RUSH reporter using the threshold function of ImageJ and to manually extract the ER object. The ER area was then measured using the "analyze particles" function with pixel sizes 50–infinity. The second part of the macro was optimized for extracting Golgi objects for each frame and for quantifying their area. The macro used ImageJ's rolling ball background subtraction algorithm followed by a median filter. A binary image was generated for each frame with the "auto threshold" function using the "moments" algorithm. Areas of binary Golgi objects were then quantified for each frame with the "analyze particles" function using pixel sizes 15–infinity. The normalized Golgi area was calculated as the ratio of Golgi compacted area at each frame and the ER area at the first frame. Normalized Golgi area for 15 control and NUCB1-KO cells were plotted for each time point as the median ± IQR. Significant differences at  $t = 22$  min with  $P < 0.05$  were analyzed using the nonparametric Mann–Whitney  $U$  test.

### Secretion assays

For the RUSH secretion assay, we followed the protocol described by Deng et al. (2018). HeLa and NUCB1-KO cells ( $10^3$ )



were seeded into six-well plates, incubated overnight, and then transfected with SS-Flag-MMP2-SBP or LyzC-Flag-SBP-eGFP for 24 h using PEI. Thereafter, the cells were incubated in DMEM serum-free medium for 45 or 60 min, and supernatants were collected and concentrated 20× using Centrifugal Filters (Amicon Ultra). The cells were then lysed using 1× PBS + 0.05% Triton A-100, and the total protein was quantified. All samples were normalized to the corresponding lysate protein concentrations. Laemmli buffer was added to a final concentration of 1×, and the samples were evaluated via SDS-PAGE and WB.

The HRP transport and secretion assay was performed as previously described (von Blume et al., 2011, 2012; Kienzle and von Blume, 2014). We seeded 125,000 HeLa or NUCB1-KO cells stably expressing SS-HRP-FLAG as technical triplicates into 12-well plates for 24 h. Before the start of HRP secretion, HeLa Brefeldin A (BFA) samples were preincubated with 10 µg/µL BFA in medium for 1 h. Cells were then washed 5× with PBS and incubated in medium with or without BFA for 4 h. Cell culture supernatants were harvested and filtered, and the cells were lysed in 0.5% Triton X-100 in PBS. Finally, 50 µl of medium and whole-cell lysis were mixed with 50 µl Liquid Substrate System solution (2,2'-azino-bis (3-ethylbenzothiazoline-6-sulfonic acid; Sigma-Aldrich, A3219). HRP activity was measured on a Magellan plate reader (Tecan Group) at 405 nm. The ratio of secreted HRP and cellular HRP was then normalized to HeLa control samples set to 100%. Normalized data from three independent experiments were plotted as mean ± SD. Significant differences with  $P < 0.05$  were analyzed using the nonparametric Kruskal-Wallis test with Dunn's multiple comparison test.

For the endogenous MMP2 secretion assay, MDA-MB-231 cells expressing MT1-MMP-mCherry were seeded into six-well plates and incubated overnight. Cells were silenced using the described siNUCB1-1 and incubated until 80% confluence was reached. At that point, cells were incubated in 2 ml L15 serum-free medium for 16–20 h, and the supernatants were collected and concentrated 20× using Centrifugal Filters (Amicon Ultra). Cells were then lysed using 1× PBS + 0.05% Triton X-100, and total protein was quantified and normalized by the corresponding cell lysate protein concentration. Samples were analyzed via SDS-PAGE and WB.

Semiquantitative analysis of band intensities was performed using Fiji, following the protocol described by (Deng et al., 2018). Normalized data from three independent experiments were plotted as the mean ± SD. Significant differences with  $P < 0.05$  were analyzed using the nonparametric Kruskal-Wallis test with Dunn's multiple comparison test.

### Enrichment of cell surface biotinylated proteins

MT1-MMP transport to the cell surface in HeLa and NUCB1-KO cells was evaluated by pulldown of biotinylated cell surface proteins using NeutrAvidin agarose beads (Pierce). Cells were cultivated as described above and seeded in 10-cm culture dishes ( $75 \times 10^3$  cells per dish) until 60% confluence. Cells were labeled with sulfo-NHS-SS-biotin (250 µg/ml) for 90 min or covered in ice-cold DPBS for control (– biotin, time 0) condition at 4°C on a platform rocker. Excess biotin was removed by washing once with ice-cold glycine in PBS (150 mM) before quenching the

biotinylation reaction by incubating in the same glycine solution for 25 min (5 ml in dish platform rocker). Cells were washed with ice-cold DPBS, collected using cell scrapers, and lysed in 1 ml lysis buffer (100 mM Tris-HCl, 150 mM NaCl, 0.1% SDS, 1% Triton, 1% deoxycholic acid, pH 7.4, + cOmplete tablets) for 30 min on ice. Cell lysates were separated from membrane and cell debris by centrifugation for 15 min at 14,000 rpm (4°C). NeutrAvidin beads were prepared for incubation by washing 2× with 0.5 ml DPBS and 0.5 ml lysis buffer (3,400 rpm, 4°C, 3 min). After determining the total protein amount per cell lysate by Bradford (absorption  $\lambda = 595$  nm), the equalized cell lysates were incubated with 150 µl NeutrAvidin bead slurry overnight at 4°C (rotating wheel). To reduce nonspecific protein binding, the beads were washed with lysis buffer (1 ml, 5×) on ice by centrifugation (3,400 rpm, 4 and 3 min). Subsequently, biotinylated proteins were eluted in 80 µl Laemmli sample buffer containing 50 mM DTT (10 min, 95°C) and analyzed by SDS-PAGE. Detection was performed via WB. Semiquantitative analysis of band intensities was performed using Fiji. Endogenous MT1-MMP band intensities were normalized to the intensity of  $\beta$ -integrin and then to the HeLa control sample at 90 min (100%). Normalized data from three independent experiments were plotted as the mean ± SD. Significant differences with  $P < 0.05$  were analyzed using a one-sample  $t$  test.

### Zymography

Gel zymography was performed as described by Toth et al. (2012). HeLa or NUCB1-KO cells ( $1.5 \times 10^5$  cells/ml) were seeded in 10-cm Petri dishes. After overnight incubation, cells were transfected with either SS-Flag-MMP2-SBP-eGFP or LyzC-Flag-SBP-eGFP using PEI. After 24 h, cells were starved for 45 min by incubating in serum-free medium containing 40 µM biotin. The supernatants were collected and concentrated 20× using Centrifugal Filters (Amicon Ultra, Ultracel 10K). Cell lysates were prepared via incubation with 300 µl zymography lysis buffer (25 mM Tris, 100 mM NaCl, and 0.1% NP-40) on ice for 15 min and centrifugation of lysates at maximal speed for 20 min. The samples were prepared by adding 1× sample buffer (zymography running buffer, 35% glycerol, 8% SDS, and 1 mg/ml Bromophenol Blue) and run on a Novex 10% Zymogram Plus (Gelatin) gel at 150 V for 80 min. Gels were briefly washed with distilled water and incubated with 100 ml 1× renaturing solution for at least 3 h. The gels were washed 3× with distilled water, incubating each time with ≥100 ml distilled water for 10 min. The water was replaced with 100 ml developing solution and incubated for 30 min at room temperature. Buffer was replaced with new 1× renaturing solution and incubated for ≥20 h at 37°C on a shaker. Finally, the gels were briefly washed with water and stained with Coomassie solution until completely dark blue. Bands appeared as sharp clear areas. If necessary, gels were briefly (<5 min) destained in a 5% methanol + 10% acetic acid solution. Semiquantitative analysis was performed with Fiji by quantifying the degraded area on the gel and setting the degraded intensity of HeLa control cells to 100% in each experiment. The degraded area of NUCB1-KO cells is expressed as percentage relative to HeLa control. Significant differences were evaluated using a one-sample  $t$  test.

## Structural visualization of NUCB1 E264Q and E316Q substitutions

The molecular graphics of the nuclear magnetic resonance structure of NUCB1 (1SNL, Research Collaboratory for Structural Bioinformatics Protein Data Bank [RCSB PDB]) were visualized and performed with UCSF Chimera (developed by the Resource for Biocomputing, Visualization, and Informatics at the University of California, San Francisco, with support from NIH P41-GM103311). The depicted rotamer was selected according to the highest probable candidate from the Dunbrack backbone-dependent rotamer library (Shapovalov and Dunbrack, 2011), and the pictures were adapted from the available model 1SNL (de Alba and Tjandra, 2004) in RCSB PDB using the UCSF Chimera software (Pettersen et al., 2004).

## Protein purification of His-tagged proteins

The expression of rHS-MMP2, rNUCB1-His, and rNUCB1-mEF1+2-His in HEK293T cells was induced by incubating the cells with DMEM serum-free medium supplemented with doxycycline and aprotinin (1 µg/ml each) for ≥20 h. For His-SUMO-MMP2 and rNUCB1-His, proteins were purified using a column packed with cOmplete His-tag purification resin from Roche, as described by Crevenna et al. (2016). For rNUCB1-mEF1+2-His purification, the supernatant was collected, concentrated 100× using Centrifugal Filters (Amicon Ultra, Ultracel 10K), and incubated with previously NaP pH 8.0 equilibrated Protino Ni-NTA agarose beads for 2 h at 4°C with rotation. The proteins were then washed and incubated with 250 mM imidazole for protein elution.

## CD spectroscopy

CD measurements were performed as described previously (Crevenna et al., 2016) with the following modifications. Measurements were performed at 4°C using 20 mM Tris + 500 mM NaCl buffer. The mean of four independent spectra (from 198 to 250 nm with 0.1-nm spacing) was recorded. CONTIN analysis was performed using CDPro. CONTIN decomposes the CD signal into six secondary structural elements: regular α-helical, distorted α-helical, regular β sheet, distorted β sheet, turn, and unordered. Reported values in the main text for the α-helical and β sheet content were the sum of regular and distorted fractions for each secondary element.

## Maleimide protein labeling

Recombinant His-SUMO-MMP2 was labeled with Cy3-NHS-Ester according to the manufacturer's instructions. After labeling, the protein was dialyzed in 20 mM Tris and 100 mM NaCl, pH 7.0, to remove excess free dye.

## AUC

Sedimentation velocity experiments were performed on an Optima XL-I analytical ultracentrifuge (Beckman) using an An 60 Ti rotor and double-sector epon center pieces. The proteins were added to a 20 mM Tris + 100 mM NaCl buffer at 0.6 and 1.6 mg/ml for rHS-MMP2 and rNUCB1-His, respectively. Buffer density and viscosity were measured using a DMA 5000 densitometer and a AMVn viscosimeter, respectively (both Anton

Paar). Fluorescently labeled protein concentration distribution was monitored at 544 nm at 50,000 rpm and 20°C. Time-derivative analysis was computed using the SEDFIT software package, v12.1b (Schuck, 2000), resulting in a  $c(s)$  distribution and an estimate of the molecular weight  $M_f$  (from the sedimentation coefficient and the diffusion coefficient, as inferred from the broadening of the sedimentation boundary, assuming all observed species share the same frictional coefficient  $f/f_0$ ).

## Ca<sup>2+</sup> influx assay

Ca<sup>2+</sup> entry into the TGN or cis-Golgi was measured as described previously (Deng et al., 2018; Lissandron et al., 2010). Ca<sup>2+</sup> measurements in the TGN or cis-Golgi were performed using a fluorescent Ca<sup>2+</sup> sensor Go-D1-cpv (which targets the TGN) or GPP130-Twitch5 (which targets the cis-Golgi). Changes in Ca<sup>2+</sup> concentration in the TGN by the Go-D1-cpv sensor were observed as changes in FRET efficiency between CFP and YFP fluorescent proteins linked by a modified CaM and CaM-binding domain. On the other hand, changes in Ca<sup>2+</sup> concentration in the cis-Golgi were observed as FRET efficiency between enhanced CFP and Citrine fluorescent proteins linked by a modified C-terminal domain of *Opsanus tau* troponin C (Thestrup et al., 2014). HeLa or NUCB1-KO cells were transfected with either Go-D1-cpv or GPP130-Twitch5 alone or with NUCB1-WT or NUCB1-EFh1+2 mutant for 24 h. Ca<sup>2+</sup> entry into the TGN or cis-Golgi were measured in Ca<sup>2+</sup>-depleted cells after incubating for 1 h at 4°C in HBSS (20 mM Hepes, Ca<sup>2+</sup>/Mg<sup>2+</sup>-free HBSS [Gibco by Life Technologies], 2 g/liter glucose, 490 µM MgCl<sub>2</sub>, and 450 µM MgSO<sub>4</sub>, 300 mOsmol/liter, pH 7.4) with 1 µM ionomycin (Abcam) and 0.5 mM EGTA; von Blume et al., 2011; Deng et al., 2018). The cells were then washed twice in HBSS + 0.5 mM EGTA followed by washing three times in HBSS only. Image acquisition was performed on a DeltaVision Elite (GE Healthcare Life Sciences) as described by Deng et al. (2018). The excitation filter (430/24), dual-band Sedat CFP/YFP beam splitter (Chroma Technology Corp.), and the emission filters (535/25 for FRET and 470/24 for CFP) were rapidly changed using an external filter wheel controlled by a motorized unit to generate the images. Fluorescent signals reflecting TGN or cis-Golgi [Ca<sup>2+</sup>] were presented as  $\Delta R/R_0$ , where  $R_0$  is the value obtained before the addition of 2.2 mM CaCl<sub>2</sub> to the cell's bathing solution. Images were acquired using softWoRx 5.5 software (GE Healthcare Life Sciences). Image analysis was conducted using a custom-made ImageJ macro based on ratiometric FRET analysis described previously (Kardash et al., 2011; Kienzle et al., 2014; Deng et al., 2018). The macro uses ImageJ's rolling ball background subtraction algorithm followed by a mean filter to smooth out the edges of the objects. A binary image was generated by the "auto threshold" function using the "moments" algorithm. FRET and CFP channel images were multiplied by the ImageCalculator plugin with their respective binary images, resulting in images that show 0 intensities outside of the threshold Golgi region while retaining intensities within the Golgi. Next, a ratio image of FRET/CFP was generated using the Ratio Plus plugin. The Golgi objects were detected using the "find maxima" function and added to the region of interest manager. The mean intensities of each region of interest were then measured in the ratio

image for each frame. The ratio values of each frame were subtracted with those in the first frame. These values were normalized to the first frame and presented as percentage  $\Delta R/R_0$  to obtain the normalized ratio values before the addition of  $\text{CaCl}_2$ .

### Invasion assay

Transwells (pore size 8  $\mu\text{m}$ ; Costar; Corning) were coated on the upper side with 50  $\mu\text{l}$  growth factor-reduced Matrigel (BD Biosciences) diluted 1:20 in L-15 medium containing 0.5% FCS and allowed to polymerize for 1 h at 37°C. Transfected cells ( $5 \times 10^4$  cells/ml) were seeded in Transwells in 100  $\mu\text{l}$  of L-15 medium containing 0.5% FCS, whereas the bottom chamber of the Transwell contained L-15 medium supplemented with 10% FCS. After 24 h of invasion, cells on the bottom of the membrane were fixed and stained with crystal violet, and six independent fields at 10 $\times$  magnification were quantified using ImageJ (v1.49s). Significant differences between the number of migrating cells in each experiment were evaluated with a paired *t* test comparing each sample to the corresponding experiment control (siControl-1 or siControl-2). *P* < 0.05 was considered significant.

### Matrix degradation of MDA-MB-231 cells

Coverslips were coated with Oregon488-conjugated gelatin (1 mg/ml; Invitrogen) followed by cross-linking with 0.5% glutaraldehyde (Carl Roth). Transfected cells ( $5 \times 10^4$  cells/ml) were seeded on coverslips, and after 5 h of incubation at 37°C, cells were fixed and nuclei were counterstained with DAPI. Imaging was performed on a confocal laser scanning microscope LSM 710 (Carl Zeiss) equipped with a Plan-Apochromat 20 $\times$ /0.8. 40 confocal images per condition were acquired using identical settings for 488 and DAPI channels. Quantitative image analysis of gelatin degradation was performed using CellProfiler software v3.0.0. Relative degraded area was defined as the measured area normalized by the average area of the siControl in each experiment. Significant differences were evaluated with a paired *t* test comparing each sample to the corresponding experiment control (siControl-1 or siControl-2). *P* < 0.05 was considered significant.

### 2D gelatin degradation assay of human primary macrophages

Gelatin (from swine; Carl Roth) was fluorescently labeled with NHS Rhodamine (Thermo Fisher Scientific) according to the method described by Chen and Ko (1994). Coverslips were coated with labeled Rhodamine-gelatin, fixed in 0.5% glutaraldehyde (Carl Roth), and washed in RPMI 1640 and culture medium. 72 h after siRNA transfection, cells were reseeded on coated coverslips at a density of  $5 \times 10^4$  cells; fixed and permeabilized 4, 6, and 8 h after seeding; and stained with Alexa Fluor 488-phalloidin. After the cells were labeled, the coverslips were mounted on Mowiol (Calbiochem) containing 1,4-diazabicyclo[2.2.2]octane (25 mg/ml; Sigma-Aldrich) as antifading reagent. Matrix degradation values were determined as 1 minus the ratio of fluorescent intensity under/around each cell using ImageJ. These values were normalized to the control (siLUC) per donor (three in total), represented as 100%, and reported in percentage relative to control. For comparison, laser intensity

was not changed between measurements. Two donors of independent experiments were analyzed, with at least eight fields of view (400–1,000 cells) per condition.

Images were acquired using confocal laser scanning microscopes (Leica DMI8 confocal point scanner equipped with a 20 $\times$  HC PL APO IMM/CORR CS2 and oil-immersion 63 $\times$  HC PL APO Oil CS2 objective and 3 $\times$  HyD, 2 $\times$  PMT, 1 $\times$  Trans-PMT detector). Acquisition and processing were performed using Leica LAS X SP8 confocal software (Leica Camera), Volocity 6.1.1 software (PerkinElmer), and ImageJ. Statistical differences between si-NUCB1 and siMMP2 samples compared with siControl were evaluated with a one-sample *t* test. Differences among si-NUCB1 and si-MMP2 degraded areas were compared with a paired *t* test for each pair of siRNAs analyzed in parallel.

### Statistical analysis

Microscopy quantification data were first evaluated for normality fit. If the data did not follow a normal distribution, we performed a nonparametric Kruskal-Wallis test with Dunn's comparison for most statistical significance evaluations. For the evaluation of statistical differences in  $\text{Ca}^{2+}$  influx assays, we used the Mann-Whitney *U* test. For semiquantitative evaluation of blots, band intensities were evaluated with ImageJ, and ratios between each band and its correspondent pulled protein band or a positive control were determined (see figure legends for more details). Statistical analyses (one-sample *t* test or paired *t* test) were performed using Prism software (GraphPad), unless otherwise stated.

### Online supplemental material

Fig. S1 shows data on MMP2-eGFP secretion and generation of CRISPR NUCB1-KO cells. Fig. S2 shows colocalization experiments with Rab GTPases, lysosomes, and LyzC. Fig. S3 details experiments with recombinant proteins. Fig. S4 depicts RUSH experiments using NUCB1-cyto and MT1-MMP-mCherry, as well as an MT1-MMP cell surface biotinylation assay. Fig. S5 shows zymography and secretion assays with different cargoes than MMPs. Table S1 lists the hits found in our MS analysis.

### Acknowledgments

We thank O. Griesbeck (Max Planck Institute of Biochemistry) for the Twitch5 sensor plasmid, Y. Maeda for the one encoding the cis-Golgi targeting sequence, A. Mordhorst for expert technical assistance, and G. Boncompain (Institute Curie, Paris, France) for generating and sharing the MT1-MMP RUSH construct.

N. Pacheco-Fernandez was funded by a Deutscher Akademischer Austauschdienst stipend (Förderprogramm ID 57129429), J. von Blume by the Perspective Program (Boehringer Ingelheim Fonds), the Deutsche Forschungsgemeinschaft (project grant BL 1186/4-1 and CRC914 (TP A09)), the National Institutes of Health, National Institute of General Medical Sciences (GM134083-01), and the Max Planck Institute of Biochemistry and the department led by R. Fässler. K. Weber was funded by a Deutsche Forschungsgemeinschaft project grant (SL: LI925/8-1). Research on MMPs in the Linder laboratory is funded by the



Deutsche Forschungsgemeinschaft (LI925/8-1; CRC877). MS, CD, and AUC analyses were provided by the Biochemistry core facility of the Max Planck Institute of Biochemistry.

The authors declare no competing financial interests.

Author contributions: Concept: N. Pacheco-Fernandez, M. Pakdel, and J. von Blume; N. Pacheco-Fernandez did experiments in Figs. 1, 2, 5, S1, S3, S4, and S5; M. Pakdel in Figs. 3, 4, 6, S1, S2, S4, and S5; B. Blank in Fig. 5; M.L. Tran in Fig. S4; T. Hecht in Fig. 5; I. Sanchez-Gonzalez in Fig. 7; K. Weber in Fig. 8; R. Gautsch in Figs. 5 and S1; G. Beck in Figs. 7 and S3; and J. von Blume in Fig. 1. Writing–Original Draft: N. Pacheco-Fernandez, B. Blank, M. Pakdel, and J. von Blume; Review and editing: N. Pacheco-Fernandez, M. Pakdel, B. Blank, M.L. Tran, T. Hecht, I. Sanchez-Gonzalez, K. Weber, R. Gautsch, G. Beck, F. Perez, A. Hausser, S. Linder and J. von Blume; Funding acquisition: N. Pacheco-Fernandez and J. von Blume; Supervision: J. von Blume.

Submitted: 9 July 2019

Revised: 29 December 2019

Accepted: 4 May 2020

## References

- Alaseem, A., K. Alhazzani, P. Dondapati, S. Alobid, A. Bishayee, and A. Rathinavelu. 2019. Matrix Metalloproteinases: A challenging paradigm of cancer management. *Semin. Cancer Biol.* 56:100–115. <https://doi.org/10.1016/j.semcancer.2017.11.008>
- Anilkumar, N., T. Uekita, J.R. Couchman, H. Nagase, M. Seiki, and Y. Itoh. 2005. Palmitoylation at Cys574 is essential for MT1-MMP to promote cell migration. *FASEB J.* 19:1326–1328. <https://doi.org/10.1096/fj.04-3651fje>
- Apte, S.S., and W.C. Parks. 2015. Metalloproteinases: A parade of functions in matrix biology and an outlook for the future. *Matrix Biol.* 44–46:1–6. <https://doi.org/10.1016/j.matbio.2015.04.005>
- Aulestia, F.J., M.T. Alonso, and J. García-Sancho. 2015. Differential calcium handling by the cis and trans regions of the Golgi apparatus. *Biochem. J.* 466:455–465. <https://doi.org/10.1042/BJ20141358>
- Barlowe, C.K., and E.A. Miller. 2013. Secretory protein biogenesis and traffic in the early secretory pathway. *Genetics*. 193:383–410. <https://doi.org/10.1534/genetics.112.142810>
- Beznoussenko, G.V., S. Parashuraman, R. Rizzo, R. Polishchuk, O. Martella, D. Di Giandomenico, A. Fusella, A. Spaar, M. Sallase, M.G. Capetrano, et al. 2014. Transport of soluble proteins through the Golgi occurs by diffusion via continuities across cisternae. *eLife*. 3. e02009. <https://doi.org/10.7554/eLife.02009>
- Boncompain, G., S. Divoux, N. Gareil, H. de Forges, A. Lescure, L. Latreche, V. Mercanti, F. Jollivet, G. Raposo, and F. Perez. 2012. Synchronization of secretory protein traffic in populations of cells. *Nat. Methods*. 9:493–498. <https://doi.org/10.1038/nmeth.1928>
- Bonito-Oliva, A., S. Barbash, T.P. Sakmar, and W.V. Graham. 2017. Nucleobindin 1 binds to multiple types of pre-fibrillar amyloid and inhibits fibrillization. *Sci. Rep.* 7:42880. <https://doi.org/10.1038/srep42880>
- Bonnans, C., J. Chou, and Z. Werb. 2014. Remodelling the extracellular matrix in development and disease. *Nat. Rev. Mol. Cell Biol.* 15:786–801. <https://doi.org/10.1038/nrm3904>
- Bravo-Cordero, J.J., R. Marrero-Diaz, D. Megías, L. Genís, A. García-Grande, M.A. García, A.G. Arroyo, and M.C. Montoya. 2007. MT1-MMP proinvasive activity is regulated by a novel Rab8-dependent exocytic pathway. *EMBO J.* 26:1499–1510. <https://doi.org/10.1038/sj.emboj.7601606>
- Brew, K., and H. Nagase. 2010. The tissue inhibitors of metalloproteinases (TIMPs): an ancient family with structural and functional diversity. *Biochim. Biophys. Acta*. 1803:55–71. <https://doi.org/10.1016/j.bbamer.2010.01.003>
- Brodeur, J., H. Larkin, R. Boucher, C. Thériault, S.C. St-Louis, H. Gagnon, and C. Lavoie. 2009. Calnuc binds to LRP9 and affects its endosomal sorting. *Traffic*. 10:1098–1114. <https://doi.org/10.1111/j.1600-0854.2009.00933.x>
- Cauwe, B., and G. Opdenakker. 2010. Intracellular substrate cleavage: a novel dimension in the biochemistry, biology and pathology of matrix metalloproteinases. *Crit. Rev. Biochem. Mol. Biol.* 45:351–423. <https://doi.org/10.3109/10409238.2010.501783>
- Chen, L., and C.P. Ko. 1994. Extension of synaptic extracellular matrix during nerve terminal sprouting in living frog neuromuscular junctions. *J. Neurosci.* 14:796–808. <https://doi.org/10.1523/JNEUROSCI.14-02-00796.1994>
- Cornfine, S., M. Himmel, P. Kopp, K. El Azzouzi, C. Wiesner, M. Krüger, T. Rudel, and S. Linder. 2011. The kinesin KIF9 and reggie/flotillin proteins regulate matrix degradation by macrophage podosomes. *Mol. Biol. Cell*. 22:202–215. <https://doi.org/10.1091/mbc.e10-05-0394>
- Crevenna, A.H., B. Blank, A. Maiser, D. Emin, J. Prescher, G. Beck, C. Kienzle, K. Bartnik, B. Habermann, M. Pakdel, et al. 2016. Secretory cargo sorting by Ca<sup>2+</sup>-dependent Cab45 oligomerization at the trans-Golgi network. *J. Cell Biol.* 213:305–314. <https://doi.org/10.1083/jcb.201601089>
- Cui, N., M. Hu, and R.A. Khalil. 2017. Biochemical and Biological Attributes of Matrix Metalloproteinases. *Prog. Mol. Biol. Transl. Sci.* 147:1–73. <https://doi.org/10.1016/bs.pmbts.2017.02.005>
- Dancourt, J., H. Zheng, F. Bottanelli, E.S. Allgeyer, J. Bewersdorf, M. Graham, X. Liu, J.E. Rothman, and G. Lavie. 2016. Small cargoes pass through synthetically glued Golgi stacks. *FEBS Lett.* 590:1675–1686. <https://doi.org/10.1002/1873-3468.12210>
- de Alba, E., and N. Tjandra. 2004. Structural studies on the Ca<sup>2+</sup>-binding domain of human nucleobindin (calnuc). *Biochemistry*. 43:10039–10049. <https://doi.org/10.1021/bi049310a>
- Deng, Y., M. Pakdel, B. Blank, E.L. Sundberg, C.G. Burd, and J. von Blume. 2018. Activity of the SPCA1 Calcium Pump Couples Sphingomyelin Synthesis to Sorting of Secretory Proteins in the Trans-Golgi Network. *Dev. Cell*. 47:464–478.e8. <https://doi.org/10.1016/j.devcel.2018.10.012>
- Deng, Y., F.E. Rivera-Molina, D.K. Toomre, and C.G. Burd. 2016. Sphingomyelin is sorted at the trans Golgi network into a distinct class of secretory vesicle. *Proc. Natl. Acad. Sci. USA*. 113:6677–6682. <https://doi.org/10.1073/pnas.1602875113>
- Deryugina, E.I., B.I. Ratnikov, Q. Yu, P.C. Baci, D.V. Rozanov, and A.Y. Strongin. 2004. Prointegrin maturation follows rapid trafficking and processing of MT1-MMP in Furin-Negative Colon Carcinoma LoVo Cells. *Traffic*. 5:627–641. <https://doi.org/10.1111/j.1600-0854.2004.00206.x>
- Dunlop, M.H., A.M. Ernst, L.K. Schroeder, D.K. Toomre, G. Lavie, and J.E. Rothman. 2017. Land-locked mammalian Golgi reveals cargo transport between stable cisternae. *Nat. Commun.* 8:432. <https://doi.org/10.1038/s41467-017-00570-z>
- Endo, K., T. Takino, H. Miyamori, H. Kinsen, T. Yoshizaki, M. Furukawa, and H. Sato. 2003. Cleavage of syndecan-1 by membrane type matrix metalloproteinase-1 stimulates cell migration. *J. Biol. Chem.* 278:40764–40770. <https://doi.org/10.1074/jbc.M306736200>
- Ernst, A.M., S.A. Syed, O. Zaki, F. Bottanelli, H. Zheng, M. Hacke, Z. Xi, F. Rivera-Molina, M. Graham, A.A. Rebane, et al. 2018. S-Palmitoylation Sorts Membrane Cargo for Anterograde Transport in the Golgi. *Dev. Cell*. 47:479–493.e7. <https://doi.org/10.1016/j.devcel.2018.10.024>
- Farquhar, M.G. 1985. Progress in unraveling pathways of Golgi traffic. *Annu. Rev. Cell Biol.* 1:447–488. <https://doi.org/10.1146/annurev.cb.01.110185.002311>
- Fernandez-Catalan, C., W. Bode, R. Huber, D. Turk, J.J. Calvete, A. Lichte, H. Tschesche, and K. Maskos. 1998. Crystal structure of the complex formed by the membrane type 1-matrix metalloproteinase with the tissue inhibitor of metalloproteinases-2, the soluble progelatinase A receptor. *EMBO J.* 17:5238–5248. <https://doi.org/10.1093/emboj/17.17.5238>
- Frittoli, E., A. Palamidessi, A. Disanza, and G. Scita. 2011. Secretory and endo/exocytic trafficking in invadopodia formation: the MT1-MMP paradigm. *Eur. J. Cell Biol.* 90:108–114. <https://doi.org/10.1016/j.ejcb.2010.04.007>
- Frittoli, E., A. Palamidessi, P. Marighetti, S. Confalonieri, F. Bianchi, C. Malinverno, G. Mazzarol, G. Viale, I. Martin-Padura, M. Garré, et al. 2014. A RAB5/RAB4 recycling circuitry induces a proteolytic invasive program and promotes tumor dissemination. *J. Cell Biol.* 206:307–328. <https://doi.org/10.1083/jcb.201403127>
- Glick, B.S., and A. Luini. 2011. Models for Golgi traffic: a critical assessment. *Cold Spring Harb. Perspect. Biol.* 3. a005215. <https://doi.org/10.1101/cshperspect.a005215>
- Glick, B.S., and V. Malhotra. 1998. The curious status of the Golgi apparatus. *Cell*. 95:883–889. [https://doi.org/10.1016/S0092-8674\(00\)81713-4](https://doi.org/10.1016/S0092-8674(00)81713-4)
- Glick, B.S., and A. Nakano. 2009. Membrane traffic within the Golgi apparatus. *Annu. Rev. Cell Dev. Biol.* 25:113–132. <https://doi.org/10.1146/annurev.cellbio.24.110707.175421>

- Gonzalez, R., H. Mohan, and S. Unniappan. 2012. Nucleobindins: bioactive precursor proteins encoding putative endocrine factors? *Gen. Comp. Endocrinol.* 176:341–346. <https://doi.org/10.1016/j.ygcen.2011.11.021>
- Gueye, Y., L. Ferhat, O. Sbati, J. Bianco, A. Ould-Yahoui, A. Bernard, E. Charrat, J.-P. Chauvin, J.-J. Risso, F. Féron, et al. 2011. Trafficking and secretion of matrix metalloproteinase-2 in olfactory ensheathing glial cells: A role in cell migration? *Glia*. 59:750–770. <https://doi.org/10.1002/glia.21146>
- Han, K.-Y., J. Dugas-Ford, M. Seiki, J.-H. Chang, and D.T. Azar. 2015. Evidence for the Involvement of MMP14 in MMP2 Processing and Recruitment in Exosomes of Corneal Fibroblasts. *Invest. Ophthalmol. Vis. Sci.* 56: 5323–5329. <https://doi.org/10.1167/iov.14-14417>
- Hannocks, M.-J., X. Zhang, H. Gerwien, A. Chashchina, M. Burmeister, E. Korpos, J. Song, and L. Sorokin. 2019. The gelatinases, MMP-2 and MMP-9, as fine tuners of neuroinflammatory processes. *Matrix Biol.* 75–76:102–113. <https://doi.org/10.1016/j.matbio.2017.11.007>
- Hansen, G.A.W., H. Vorum, C. Jacobsen, and B. Honoré. 2009. Calumenin but not reticulocalbin forms a Ca<sup>2+</sup>-dependent complex with thrombospondin-1. A potential role in haemostasis and thrombosis. *Mol. Cell. Biochem.* 320:25–33. <https://doi.org/10.1007/s11010-008-9895-1>
- Honoré, B. 2009. The rapidly expanding CREC protein family: members, localization, function, and role in disease. *BioEssays*. 31:262–277. <https://doi.org/10.1002/bies.200800186>
- Honoré, B., and H. Vorum. 2000. The CREC family, a novel family of multiple EF-hand, low-affinity Ca(2+)-binding proteins localised to the secretory pathway of mammalian cells. *FEBS Lett.* 466:11–18. [https://doi.org/10.1016/S0014-5793\(99\)01780-9](https://doi.org/10.1016/S0014-5793(99)01780-9)
- Itoh, Y. 2015. Membrane-type matrix metalloproteinases: Their functions and regulations. *Matrix Biol.* 44–46:207–223. <https://doi.org/10.1016/j.matbio.2015.03.004>
- Jacob, A., J. Jing, J. Lee, P. Schedin, S.M. Gilbert, A.A. Peden, J.R. Junutula, and R. Prekeris. 2013. Rab40b regulates trafficking of MMP2 and MMP9 during invadopodia formation and invasion of breast cancer cells. *J. Cell Sci.* 126:4647–4658. <https://doi.org/10.1242/jcs.126573>
- Jacob, A., E. Linklater, B.A. Bayless, T. Lyons, and R. Prekeris. 2016. The role and regulation of Rab40b-Tks5 complex during invadopodia formation and cancer cell invasion. *J. Cell Sci.* 129:4341–4353. <https://doi.org/10.1242/jcs.193904>
- Jobin, P.G., G.S. Butler, and C.M. Overall. 2017. New intracellular activities of matrix metalloproteinases shine in the moonlight. *Biochim. Biophys. Acta Mol. Cell Res.* 1864(11 Pt A):2043–2055. <https://doi.org/10.1016/j.bbamcr.2017.05.013>
- Kajiho, H., Y. Kajiho, E. Frittoli, S. Confalonieri, G. Bertalot, G. Viale, P.P. Di Fiore, A. Oldani, M. Garre, G.V. Beznoussenko, et al. 2016. RAB2A controls MT1-MMP endocytic and E-cadherin polarized Golgi trafficking to promote invasive breast cancer programs. *EMBO Rep.* 17: 1061–1080. <https://doi.org/10.15252/embr.201642032>
- Kanuru, M., and G.K. Aradhyam. 2017. Chaperone-like Activity of Calnuc Prevents Amyloid Aggregation. *Biochemistry*. 56:149–159. <https://doi.org/10.1021/acs.biochem.6b00660>
- Kanuru, M., J.J. Samuel, L.M. Balivada, and G.K. Aradhyam. 2009. Ion-binding properties of Calnuc, Ca<sup>2+</sup> versus Mg<sup>2+</sup>—Calnuc adopts additional and unusual Ca<sup>2+</sup>-binding sites upon interaction with G-protein. *FEBS J.* 276:2529–2546. <https://doi.org/10.1111/j.1742-4658.2009.06977.x>
- Kapoor, N., R. Gupta, S.T. Menon, E. Folta-Stogniew, D.P. Raleigh, and T.P. Sakmar. 2010. Nucleobindin 1 is a calcium-regulated guanine nucleotide dissociation inhibitor of Galphai1. *J. Biol. Chem.* 285:31647–31660. <https://doi.org/10.1074/jbc.M110.148429>
- Kardash, E., J. Bandemer, and E. Raz. 2011. Imaging protein activity in live embryos using fluorescence resonance energy transfer biosensors. *Nat. Protoc.* 6:1835–1846. <https://doi.org/10.1038/nprot.2011.395>
- Kean, M.J., K.C. Williams, M. Skalski, D. Myers, A. Burtnik, D. Foster, and M.G. Coppelino. 2009. VAMP3, syntaxin-13 and SNAP23 are involved in secretion of matrix metalloproteinases, degradation of the extracellular matrix and cell invasion. *J. Cell Sci.* 122:4089–4098. <https://doi.org/10.1242/jcs.052761>
- Kessenbrock, K., V. Plaks, and Z. Werb. 2010. Matrix metalloproteinases: regulators of the tumor microenvironment. *Cell*. 141:52–67. <https://doi.org/10.1016/j.cell.2010.03.015>
- Khokha, R., A. Murthy, and A. Weiss. 2013. Metalloproteinases and their natural inhibitors in inflammation and immunity. *Nat. Rev. Immunol.* 13:649–665. <https://doi.org/10.1038/nri3499>
- Kienzie, C., and J. von Blume. 2014. Secretory cargo sorting at the trans-Golgi network. *Trends Cell Biol.* 24:584–593. <https://doi.org/10.1016/j.tcb.2014.04.007>
- Kienzie, C., N. Basnet, A.H. Crevenna, G. Beck, B. Habermann, N. Mizuno, and J. von Blume. 2014. Cofilin recruits F-actin to SPCA1 and promotes Ca<sup>2+</sup>-mediated secretory cargo sorting. *J. Cell Biol.* 206:635–654. <https://doi.org/10.1083/jcb.201311052>
- Könnecke, H., and I. Bechmann. 2013. The role of microglia and matrix metalloproteinases involvement in neuroinflammation and gliomas. *Clin. Dev. Immunol.* 2013. 914104. <https://doi.org/10.1155/2013/914104>
- Kurokawa, K., H. Osakada, T. Kojidani, M. Waga, Y. Suda, H. Asakawa, T. Haraguchi, and A. Nakano. 2019. Visualization of secretory cargo transport within the Golgi apparatus. *J. Cell Biol.* 218:1602–1618. <https://doi.org/10.1083/jcb.201807194>
- Larkin, H., S. Costantino, M.N.J. Seaman, and C. Lavoie. 2016. Calnuc Function in Endosomal Sorting of Lysosomal Receptors. *Traffic*. 17:416–432. <https://doi.org/10.1111/tra.12374>
- Lavieu, G., H. Zheng, and J.E. Rothman. 2013. Stapled Golgi cisternae remain in place as cargo passes through the stack. *eLife*. 2. e00558. <https://doi.org/10.7554/eLife.00558>
- Lavoie, C., T. Meerloo, P. Lin, and M.G. Farquhar. 2002. Calnuc, an EF-hand Ca(2+)-binding protein, is stored and processed in the Golgi and secreted by the constitutive-like pathway in AtT20 cells. *Mol. Endocrinol.* 16:2462–2474. <https://doi.org/10.1210/me.2002-0079>
- Leung, A.K.-W., N. Ramesh, C. Vogel, and S. Unniappan. 2019. Nucleobindins and encoded peptides: From cell signaling to physiology. *Adv. Protein Chem. Struct. Biol.* 116:91–133. <https://doi.org/10.1016/bs.apcsb.2019.02.001>
- Lin, P., H. Le-Niculescu, R. Hofmeister, J.M. McCaffery, M. Jin, H. Henne-mann, T. McQuistan, L. De Vries, and M.G. Farquhar. 1998. The mammalian calcium-binding protein, nucleobindin (CALNUC), is a Golgi resident protein. *J. Cell Biol.* 141:1515–1527. <https://doi.org/10.1083/jcb.141.7.1515>
- Lin, P., Y. Yao, R. Hofmeister, R.Y. Tsien, and M.G. Farquhar. 1999. Over-expression of CALNUC (nucleobindin) increases agonist and thapsigargin releasable Ca<sup>2+</sup> storage in the Golgi. *J. Cell Biol.* 145:279–289. <https://doi.org/10.1083/jcb.145.2.279>
- Linder, S., and G. Scita. 2015. RABGTPases in MT1-MMP trafficking and cell invasion: Physiology versus pathology. *Small GTPases*. 6:145–152. <https://doi.org/10.4161/21541248.2014.985484>
- Linder, S., and C. Wiesner. 2015. Tools of the trade: podosomes as multipurpose organelles of monocytic cells. *Cell. Mol. Life Sci.* 72:121–135. <https://doi.org/10.1007/s00018-014-1731-z>
- Linder, S., and C. Wiesner. 2016. Feel the force: Podosomes in mechanosensing. *Exp. Cell Res.* 343:67–72. <https://doi.org/10.1016/j.yexcr.2015.11.026>
- Lissandron, V., P. Podini, P. Pizzo, and T. Pozzan. 2010. Unique characteristics of Ca<sup>2+</sup> homeostasis of the trans-Golgi compartment. *Proc. Natl. Acad. Sci. USA*. 107:9198–9203. <https://doi.org/10.1073/pnas.1004702107>
- Maeda, Y., and T. Kinoshita. 2010. The Acidic Environment of the Golgi Is Critical for Glycosylation and Transport. *Methods in Enzymology*. 480: 495–510. [https://doi.org/10.1016/S0076-6879\(10\)80022-9](https://doi.org/10.1016/S0076-6879(10)80022-9)
- Malhotra, V., T. Serafini, L. Orci, J.C. Shepherd, and J.E. Rothman. 1989. Purification of a novel class of coated vesicles mediating biosynthetic protein transport through the Golgi stack. *Cell*. 58:329–336. [https://doi.org/10.1016/0092-8674\(89\)90847-7](https://doi.org/10.1016/0092-8674(89)90847-7)
- Margulis, N.G., J.D. Wilson, C.M. Bentivoglio, N. Dhungel, A.D. Gitler, and C. Barlowe. 2016. Analysis of COPII Vesicles Indicates a Role for the Emp47-Ssp120 Complex in Transport of Cell Surface Glycoproteins. *Traffic*. 17:191–210. <https://doi.org/10.1111/tra.12356>
- McCaughy, J., and D.J. Stephens. 2018. COPII-dependent ER export in animal cells: adaptation and control for diverse cargo. *Histochem. Cell Biol.* 150: 119–131. <https://doi.org/10.1007/s00418-018-1689-2>
- Micaroni, M., G. Perinetti, D. Di Giandomenico, K. Bianchi, A. Spaar, and A.A. Mironov. 2010. Synchronous intra-Golgi transport induces the release of Ca<sup>2+</sup> from the Golgi apparatus. *Exp. Cell Res.* 316:2071–2086. <https://doi.org/10.1016/j.yexcr.2010.04.024>
- Mironov, A.A., and G.V. Beznoussenko. 2019. Models of Intracellular Transport: Pros and Cons. *Front. Cell Dev. Biol.* 7:146. <https://doi.org/10.3389/fcell.2019.00146>
- Missiaen, L., L. Raeymaekers, L. Dode, J. Vanoevelen, K. Van Baelen, J.B. Parys, G. Callewaert, H. De Smedt, S. Segaut, and F. Wuytack. 2004. SPCA1 pumps and Hailey-Hailey disease. *Biochem. Biophys. Res. Commun.* 322:1204–1213. <https://doi.org/10.1016/j.bbrc.2004.07.128>
- Miura, K., Y. Kurosawa, and Y. Kanai. 1994. Calcium-binding activity of nucleobindin mediated by an EF hand moiety. *Biochem. Biophys. Res. Commun.* 199:1388–1393. <https://doi.org/10.1006/bbrc.1994.1384>
- Monteiro, P., C. Rossé, A. Castro-Castro, M. Irondelle, E. Lagoutte, P. Paul-Gilloteaux, C. Desnos, E. Formstecher, F. Darchen, D. Perrais, et al. 2013. Endosomal WASH and exocyst complexes control exocytosis of

- MT1-MMP at invadopodia. *J. Cell Biol.* 203:1063–1079. <https://doi.org/10.1083/jcb.201306162>
- Murphy, D.A., and S.A. Courtneidge. 2011. The ‘ins’ and ‘outs’ of podosomes and invadopodia: characteristics, formation and function. *Nat. Rev. Mol. Cell Biol.* 12:413–426. <https://doi.org/10.1038/nrm3141>
- Orci, L., B.S. Glick, and J.E. Rothman. 1986. A new type of coated vesicular carrier that appears not to contain clathrin: its possible role in protein transport within the Golgi stack. *Cell.* 46:171–184. [https://doi.org/10.1016/0092-8674\(86\)90734-8](https://doi.org/10.1016/0092-8674(86)90734-8)
- Pettersen, E.F., T.D. Goddard, C.C. Huang, G.S. Couch, D.M. Greenblatt, E.C. Meng, and T.E. Ferrin. 2004. UCSF Chimera—a visualization system for exploratory research and analysis. *J. Comput. Chem.* 25:1605–1612. <https://doi.org/10.1002/jcc.20084>
- Pizzo, P., V. Lissandron, and T. Pozzan. 2010. The trans-golgi compartment: A new distinct intracellular Ca store. *Commun. Integr. Biol.* 3:462–464. <https://doi.org/10.4161/cib.3.5.12473>
- Poincloux, R., F. Lizárraga, and P. Chavrier. 2009. Matrix invasion by tumour cells: a focus on MT1-MMP trafficking to invadopodia. *J. Cell Sci.* 122: 3015–3024. <https://doi.org/10.1242/jcs.034561>
- Porat, A., and Z. Elazar. 2000. Regulation of intra-Golgi membrane transport by calcium. *J. Biol. Chem.* 275:29233–29237. <https://doi.org/10.1074/jbc.M005316200>
- Rayl, M., M. Truitt, A. Held, J. Sargeant, K. Thorsen, and J.C. Hay. 2016. Penta- EF-hand protein peflin is a negative regulator of ER-to-Golgi transport. *PLoS One*. 11. e0157227. <https://doi.org/10.1371/journal.pone.0157227>
- Reichel, C.A., M. Rehberg, P. Bihari, C.M. Moser, S. Linder, A. Khandoga, and F. Krombach. 2008. Gelatinases mediate neutrophil recruitment in vivo: evidence for stimulus specificity and a critical role in collagen IV remodeling. *J. Leukoc. Biol.* 83:864–874. <https://doi.org/10.1189/jlb.1007666>
- Sakurai-Yageta, M., C. Cecchi, G. Le Dez, J.B. Sibarita, L. Daviet, J. Camonis, C. D'Souza-Schorey, and P. Chavrier. 2008. The interaction of IQGAP1 with the exocyst complex is required for tumor cell invasion downstream of Cdc42 and RhoA. *J. Cell Biol.* 181:985–998. <https://doi.org/10.1083/jcb.200709076>
- Sbai, O., L. Ferhat, A. Bernard, Y. Gueye, A. Ould-Yahoui, S. Thiolloy, E. Charrat, G. Charton, E. Tremblay, J.-J. Risso, et al. 2008. Vesicular trafficking and secretion of matrix metalloproteinases-2, -9 and tissue inhibitor of metalloproteinases-1 in neuronal cells. *Mol. Cell. Neurosci.* 39:549–568. <https://doi.org/10.1016/j.mcn.2008.08.004>
- Sbai, O., A. Ould-Yahoui, L. Ferhat, Y. Gueye, A. Bernard, E. Charrat, A. Mehanna, J.-J. Risso, J.-P. Chauvin, E. Fenouillet, et al. 2010. Differential vesicular distribution and trafficking of MMP-2, MMP-9, and their inhibitors in astrocytes. *Glia*. 58:344–366. <https://doi.org/10.1002/glia.20927>
- Scherer, P.E., G.Z. Lederkremer, S. Williams, M. Fogliano, G. Baldini, and H.F. Lodish. 1996. Cab45, a novel (Ca<sup>2+</sup>)-binding protein localized to the Golgi lumen. *J. Cell Biol.* 133:257–268. <https://doi.org/10.1083/jcb.133.2.257>
- Schuck, P.. 2000. Size-distribution analysis of macromolecules by sedimentation velocity ultracentrifugation and lamm equation modeling. *Biophys. J.* 78:1606–1619. [https://doi.org/10.1016/S0006-3495\(00\)76713-0](https://doi.org/10.1016/S0006-3495(00)76713-0)
- Shapovalov, M.V., and R.L. Dunbrack, Jr.. 2011. A smoothed backbone-dependent rotamer library for proteins derived from adaptive kernel density estimates and regressions. *Structure*. 19:844–858. <https://doi.org/10.1016/j.str.2011.03.019>
- Shaverdashvili, K., P. Wong, J. Ma, K. Zhang, I. Osman, and B. Bedogni. 2014. MT1-MMP modulates melanoma cell dissemination and metastasis through activation of MMP2 and RAC1. *Pigment Cell Melanoma Res.* 27: 287–296. <https://doi.org/10.1111/pcmr.12201>
- Shimoda, M., and R. Khokha. 2017. Metalloproteinases in extracellular vesicles. *Biochim. Biophys. Acta Mol. Cell Res.* 1864(11 Pt A):1989–2000. <https://doi.org/10.1016/j.bbamer.2017.05.027>
- Tallant, C., A. Marrero, and F.X. Gomis-Rüth. 2010. Matrix metalloproteinases: fold and function of their catalytic domains. *Biochim. Biophys. Acta*. 1803:20–28. <https://doi.org/10.1016/j.bbamer.2009.04.003>
- Theocharis, A.D., D. Manou, and N.K. Karamanos. 2019. The extracellular matrix as a multitasking player in disease. *FEBS J.* 286:2830–2869. <https://doi.org/10.1111/febs.14818>
- Thestrup, T., J. Litzlbauer, I. Bartholomäus, M. Mues, L. Russo, H. Dana, Y. Kovalchuk, Y. Liang, G. Kalamakis, Y. Laukat, et al. 2014. Optimized ratiometric calcium sensors for functional in vivo imaging of neurons and T lymphocytes. *Nat. Methods*. 11:175–182. <https://doi.org/10.1038/nmeth.2773>
- Ton, V.K., and R. Rao. 2004. Functional expression of heterologous proteins in yeast: insights into Ca<sup>2+</sup> signaling and Ca<sup>2+</sup>-transporting ATPases. *Am. J. Physiol. Cell Physiol.* 287:C580–C589. <https://doi.org/10.1152/ajpcell.00135.2004>
- Toth, M., A. Sohail, and R. Fridman. 2012. Assessment of Gelatinases (MMP-2 and MMP-9) by Gelatin Zymography. In *Metastasis Research Protocols*. M. Dwek, S.A. Brooks, and U. Schumacher, editors. Humana Press, Totowa, NJ, pp. 121–135. [https://doi.org/10.1007/978-1-61779-854-2\\_8](https://doi.org/10.1007/978-1-61779-854-2_8)
- Tulke, S., P. Williams, A. Helysaz, E. Ilegems, M. Wendel, and C. Broberger. 2016. Nucleobindin 1 (NUCB1) is a Golgi-resident marker of neurons. *Neuroscience*. 314:179–188. <https://doi.org/10.1016/j.neuroscience.2015.11.062>
- Tyanova, S., T. Temu, P. Sinitcyn, A. Carlson, M.Y. Hein, T. Geiger, M. Mann, and J. Cox. 2016. The Perseus computational platform for comprehensive analysis of (prote)omics data. *Nat. Methods*. 13:731–740. <https://doi.org/10.1038/nmeth.3901>
- Van Goethem, E., R. Poincloux, F. Gauffre, I. Maridonneau-Parini, and V. Le Cabec. 2010. Matrix architecture dictates three-dimensional migration modes of human macrophages: differential involvement of proteases and podosome-like structures. *J. Immunol.* 184:1049–1061. <https://doi.org/10.4049/jimmunol.0902223>
- Vandoreen, J., P.E. Van den Steen, and G. Opdenakker. 2013. Biochemistry and molecular biology of gelatinase B or matrix metalloproteinase-9 (MMP-9): the next decade. *Crit. Rev. Biochem. Mol. Biol.* 48:222–272. <https://doi.org/10.3109/10409238.2013.770819>
- Vanoevelen, J., L. Raeymaekers, J.B. Parys, H. De Smedt, K. Van Baelen, G. Callewaert, F. Wuytack, and L. Missiaen. 2004. Inositol trisphosphate producing agonists do not mobilize the thapsigargin-insensitive part of the endoplasmic-reticulum and Golgi Ca<sup>2+</sup> store. *Cell Calcium*. 35: 115–121. <https://doi.org/10.1016/j.ceca.2003.08.003>
- Vanoevelen, J., L. Raeymaekers, L. Dode, J.B. Parys, H. De Smedt, G. Callewaert, F. Wuytack, and L. Missiaen. 2005. Cytosolic Ca<sup>2+</sup> signals depending on the functional state of the Golgi in HeLa cells. *Cell Calcium*. 38:489–495. <https://doi.org/10.1016/j.ceca.2005.07.003>
- von Blume, J., A.-M. Alleaume, G. Cantero-Recasens, A. Curwin, A. Carreras-Sureda, T. Zimmermann, J. van Galen, Y. Wakana, M.A. Valverde, and V. Malhotra. 2011. ADF/cofilin regulates secretory cargo sorting at the TGN via the Ca<sup>2+</sup> ATPase SPCA1. *Dev. Cell*. 20:652–662. <https://doi.org/10.1016/j.devcel.2011.03.014>
- von Blume, J., A.-M. Alleaume, C. Kienzie, A. Carreras-Sureda, M. Valverde, and V. Malhotra. 2012. Cab45 is required for Ca<sup>2+</sup>-dependent secretory cargo sorting at the trans-Golgi network. *J. Cell Biol.* 199:1057–1066. <https://doi.org/10.1083/jcb.201207180>
- Vorum, H., H. Hager, B.M. Christensen, S. Nielsen, and B. Honoré. 1999. Human calumenin localizes to the secretory pathway and is secreted to the medium. *Exp. Cell Res.* 248:473–481. <https://doi.org/10.1006/excr.1999.4431>
- Wiech, H., B.M. Geier, T. Paschke, A. Spang, K. Grein, J. Steinkötter, M. Melkonian, and E. Schiebel. 1996. Characterization of green alga, yeast, and human centrins. Specific subdomain features determine functional diversity. *J. Biol. Chem.* 271:22453–22461. <https://doi.org/10.1074/jbc.271.37.22453>
- Wiesner, C., K. El Azzouzi, and S. Linder. 2013. A specific subset of RabGTPases controls cell surface exposure of MT1-MMP, extracellular matrix degradation and three-dimensional invasion of macrophages. *J. Cell Sci.* 126:2820–2833. <https://doi.org/10.1242/jcs.122358>
- Wiesner, C., J. Faix, M. Himmel, F. Bentzien, and S. Linder. 2010. KIF5B and KIF3A/KIF3B kinesins drive MT1-MMP surface exposure, CD44 shedding, and extracellular matrix degradation in primary macrophages. *Blood*. 116:1559–1569. <https://doi.org/10.1182/blood-2009-12-257089>



## Supplemental material

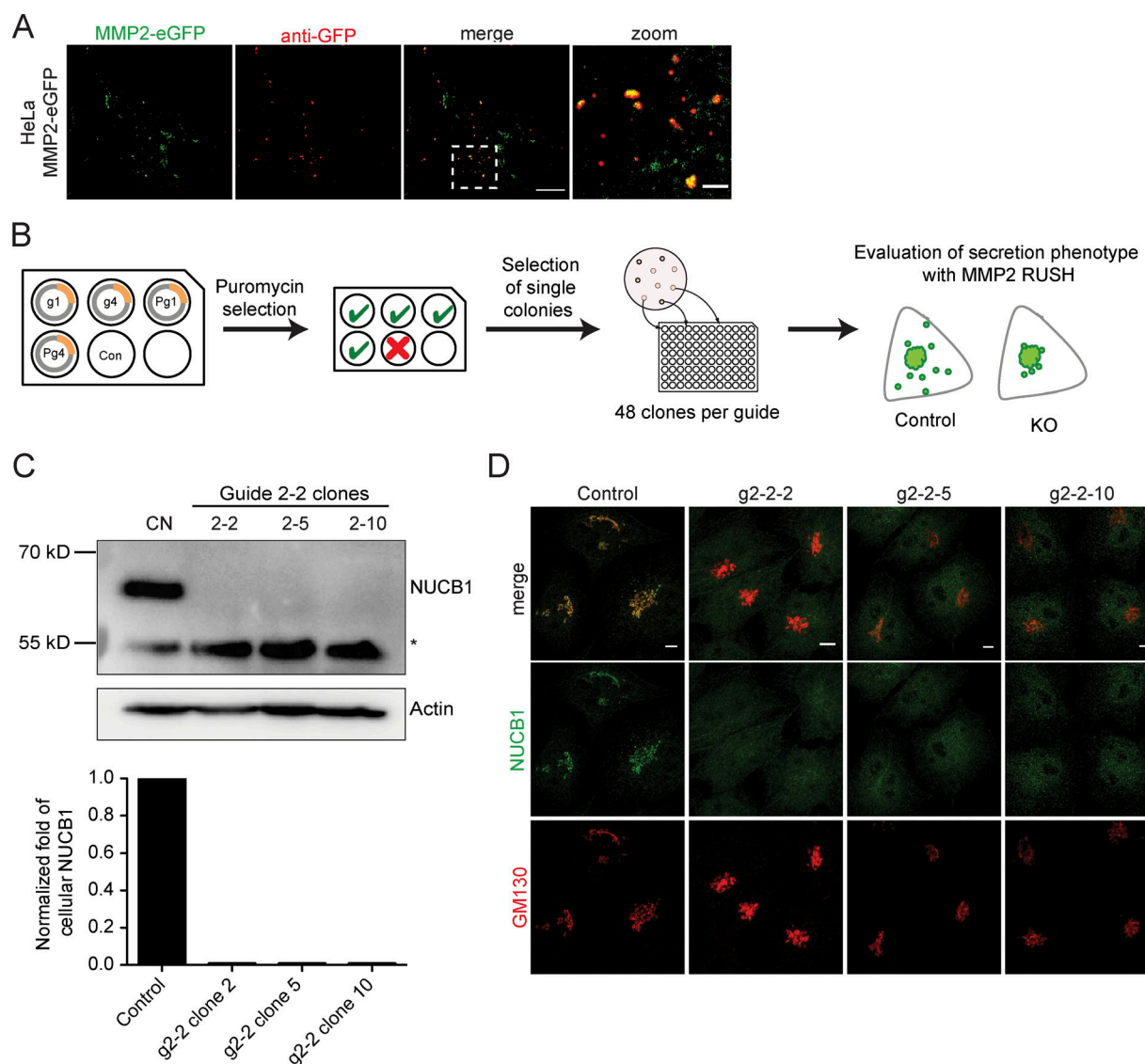


Figure S1. **MMP2-eGFP secretion and evaluation of CRISPR NUCB1-KO clones.** (A) HeLa cells stably expressing SS-MMP2-eGFP were seeded on glass slides and incubated at 37°C for 3 d to evaluate MMP2-eGFP secretion. After fixation, cells were incubated with GFP antibody and Alexa Fluor 594. Confocal fluorescence images show colocalization of MMP2-eGFP and GFP antibody of nonpermeabilized cells, evidencing secretion of MMP2-eGFP to the extracellular space. Scale bars, 10  $\mu$ m; zoom bar, 2  $\mu$ m. (B and C) NUCB1-KO cells were generated using the CRISPR-Cas9 system with three different gRNAs and selection of single colonies. After puromycin selection, three NUCB1-KO clones were identified by WB (B) and later confirmed by immunofluorescence (C). \*, unspecific band; KO, HeLa NUCB1-KO cells; CN, HeLa control. Semiquantitative analysis shows normalized NUCB1-to- $\beta$ -actin signal.

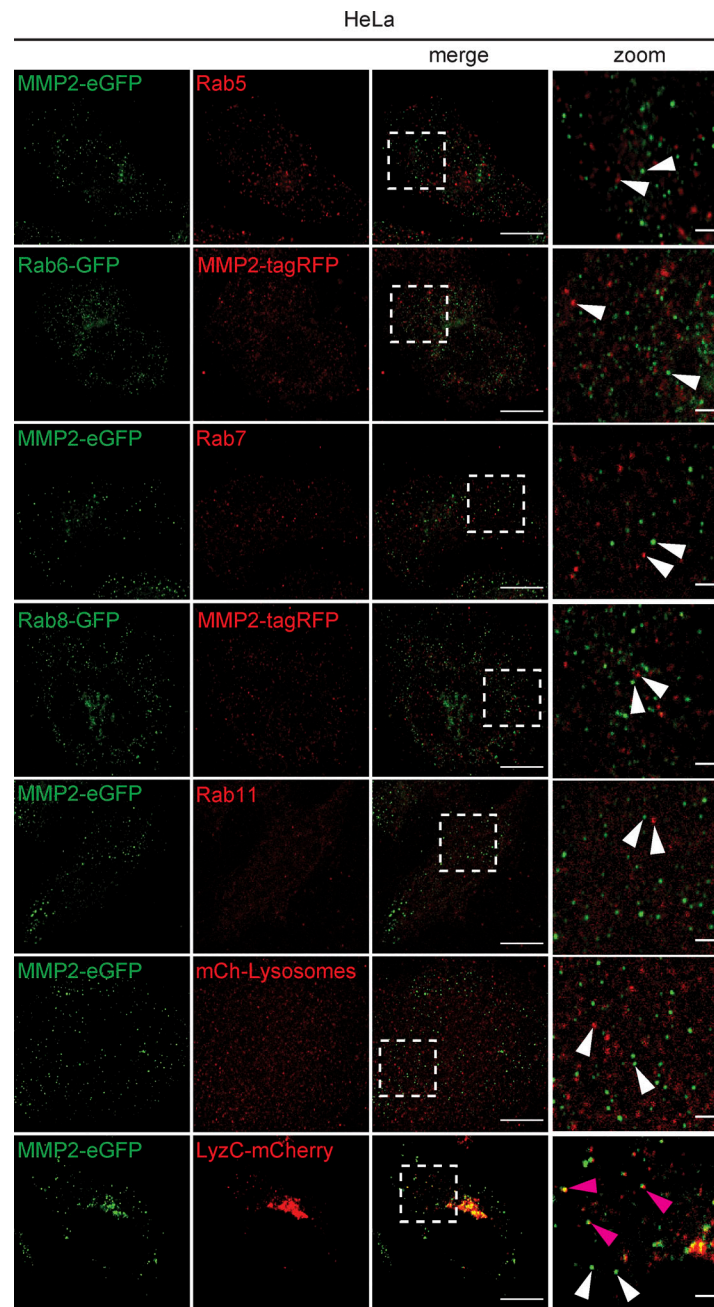
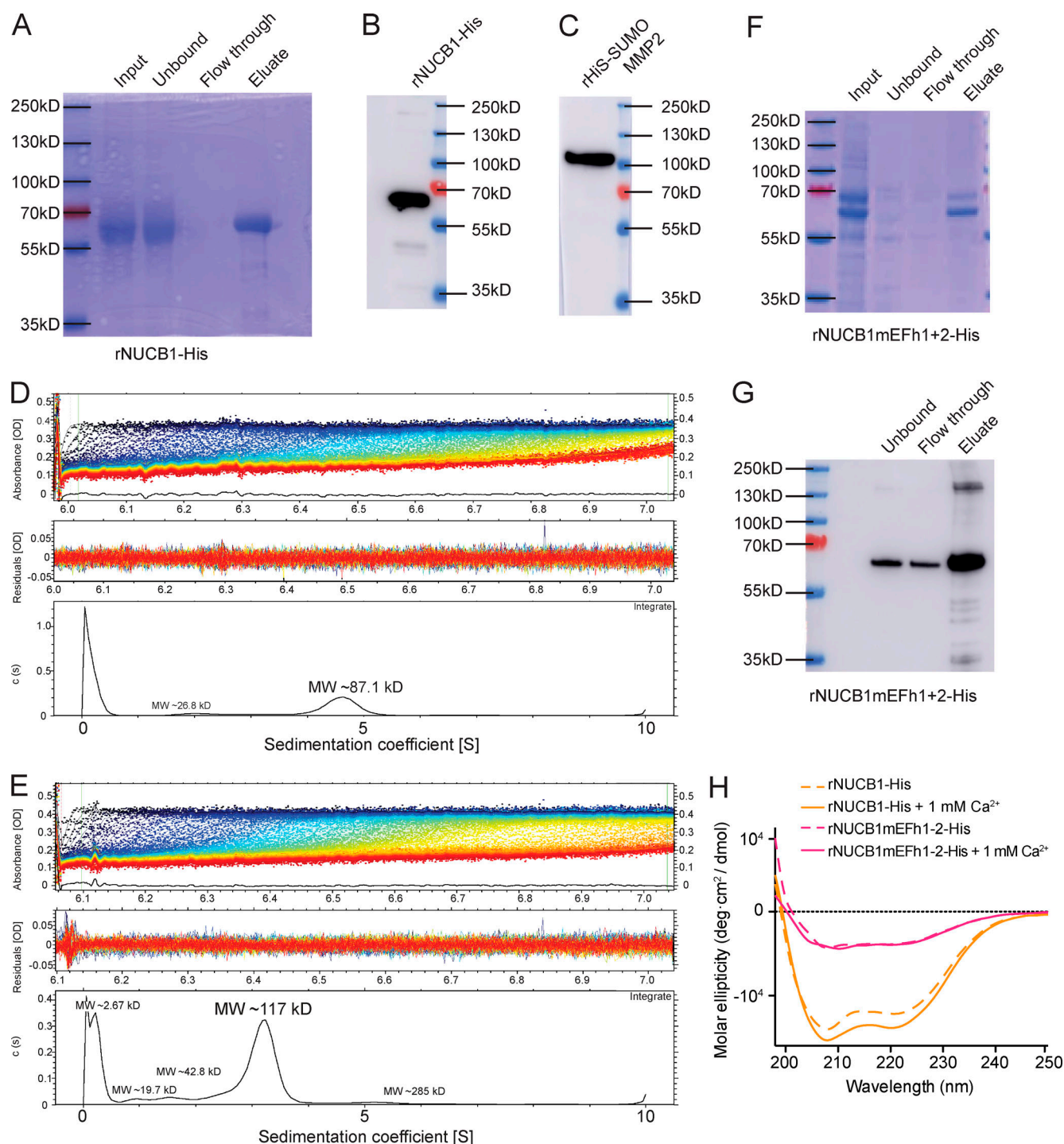
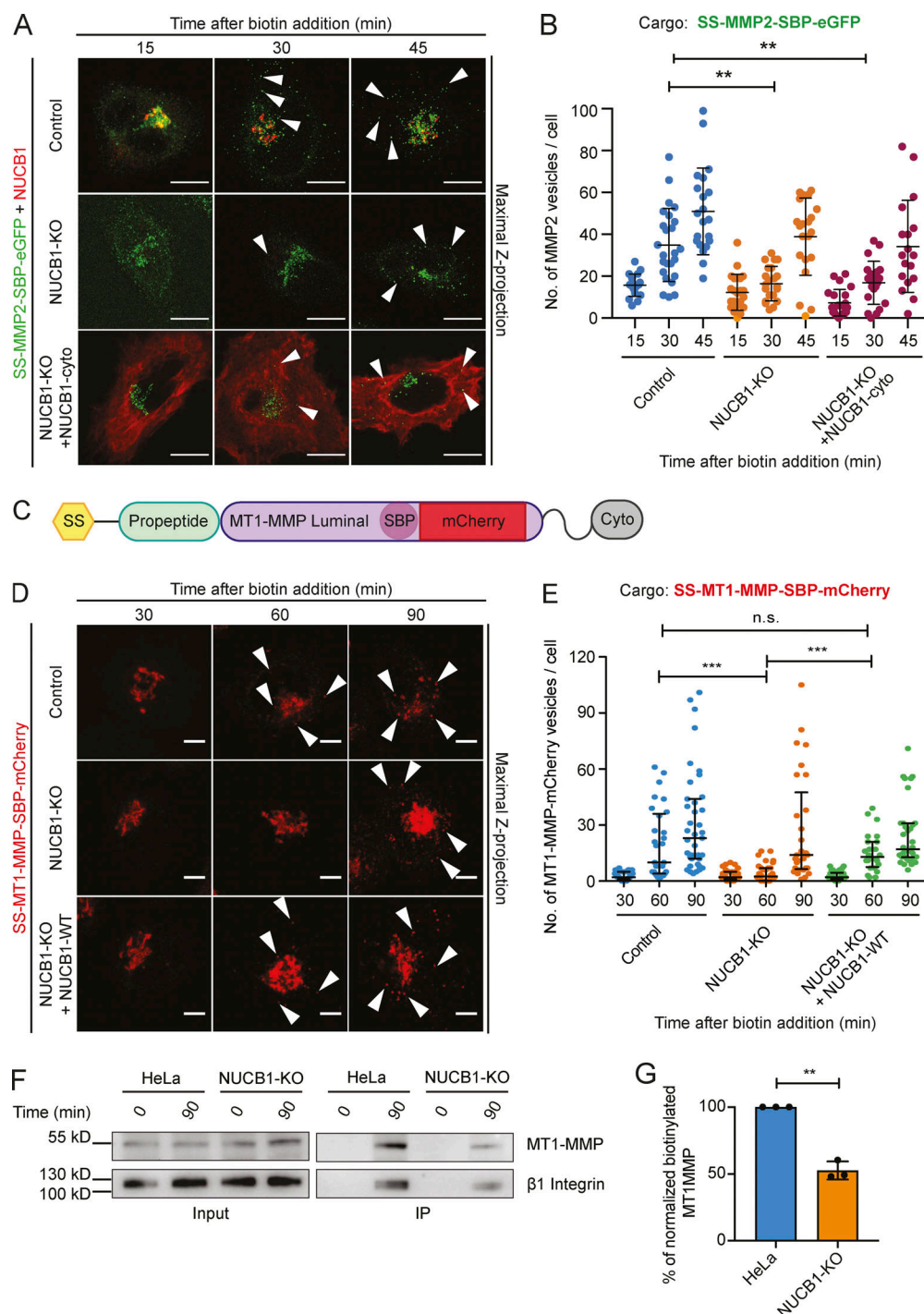


Figure S2. **MMP2 is partially sorted in LyzC-positive secretory vesicles.** HeLa cells expressing MMP2-eGFP were immunolabeled with a-Rab5, a-Rab7, or Rab11 antibodies (red). MMP2-eGFP-expressing cells were cotransfected with mCherry (mCh)-lysosomes or LyzC-mCherry to label lysosomes or LyzC-positive secretory vesicles, respectively. Rab6-GFP or Rab8-GFP constructs were cotransfected with MMP2-tagRFP. Images were acquired by confocal microscopy. White arrowheads point to distinct vesicles; magenta arrowheads point to colocalizing vesicles. Bars, 10  $\mu$ m; zoom, 2  $\mu$ m.



**Figure S3. Protein purification and evaluation of the direct interaction between MMP2 and NUCB1.** (A) Coomassie-stained SDS-PAGE for the evaluation of His-tag purified recombinant NUCB1-His (rNUCB1-His). (B) Anti-NUCB1 WB analysis of the elution fraction shown in line 4 from A. (C) WB analysis of purified His-SUMO-MMP2 using MMP2 antibody. (D) Recombinant His-SUMO-MMP2 (rHS-MMP2) was bioconjugated with Cy3 via maleimide labeling and subsequently analyzed by AUC. The lowest panel shows peak of sedimentation of rHS-MMP2 at 4.705 S. (E) AUC profile of rHis-SUMO-MMP2-Cy3 and NUCB1-His. The lowest panel shows a peak at 3.189 S, indicating a change in the sedimentation velocity associated to a direct interaction of NUCB1 and MMP2. (F) Coomassie-stained SDS-PAGE of purified His-tagged NUCB1  $\text{Ca}^{2+}$  binding mutant (rNUCB1mEFh1+2). (G) WB analysis of the elution fraction shown in line 4 of F using NUCB1 antibody. (H) CD measurement of rNUCB1-His and rNUCB1mEFh1+2-His under presence or absence of 1 mM  $\text{Ca}^{2+}$ . rNUCB1-mEFh1+2 molar ellipticity is lower compared with rNUCB1-His. Evaluation of the CD spectra using CONTIN (Wiech et al., 1996) showed an increase in rNUCB1-His  $\alpha$ -helicity upon  $\text{Ca}^{2+}$  addition (from 0.385 to 0.413) that was not observed in rNUCB1-mEFh1+2 (from 0.256 to 0.147). Instead, an increase in  $\beta$ -sheet content (from 0.151 to 0.322) was observed. These findings are in accordance with the results described by de Alba and Tjandra (2004).





**Figure S4. MMP2 IG trafficking is exclusively dependent on Golgi-localized NUCB1, which also impairs IG trafficking of MT1-MMP.** (A) HeLa or NUCB1-KO cells expressing SS-SBP-MMP2-eGFP alone or with a cytosolic variant of NUCB1 lacking its SS (NUCB1-cyto) were fixed after 0, 15, 30, and 45 min of biotin incubation. Maximal Z-projection analysis of confocal microscopy images shows no differences in MMP2 trafficking of NUCB1-cyto transfected cells compared with NUCB1-KO cells (arrowheads). Scale bars, 10  $\mu$ m. (B) Quantification of cytoplasmic MMP2 vesicles from cells in A.  $n > 18$  cells; mean  $\pm$  SD; two independent experiments. Significant differences with  $P < 0.05$  were analyzed via nonparametric Kruskal-Wallis test with Dunn's multiple comparison, \*\*,  $P < 0.01$ . (C) mCherry-tagged MT1-MMP RUSH construct (SS-MT1-MMP-SBP-mCh). Cyto, cytosolic domain. (D) Confocal fluorescence images of HeLa or NUCB1-KO cells transfected with or without NUCB1-WT and fixed after 30, 60, and 90 min of biotin incubation. Arrowheads, cytoplasmic vesicles. Scale bars, 5  $\mu$ m. (E) Quantification of cytoplasmic vesicles observed in A.  $n = 24$  cells; two independent experiments; median  $\pm$  IQR; \*\*\*,  $P < 0.001$ ; n.s., non-significant. (F) Cell surface biotinylation assay coupled with streptavidin pull-down. HeLa or NUCB1-KO cells were untreated (time 0) or incubated with sulfo-NHS-Biotin for 90 min to label cell surface proteins, and then pulled down with Neutravidin beads. WB analysis shows a reduction in the amount of endogenous active MT1-MMP at the surface of NUCB1-KO cells compared with HeLa control.  $\beta$ -1 integrin was used as loading control. (G) Semiquantitative analysis of surface labeled active MT1-MMP from F represented as % of normalized MT1-MMP intensity to  $\beta$ -1 integrin in comparison to control (100%).  $n = 3$  independent experiments; one-sample  $t$  test, \*\*,  $P < 0.01$ . Bars, mean  $\pm$  SD.

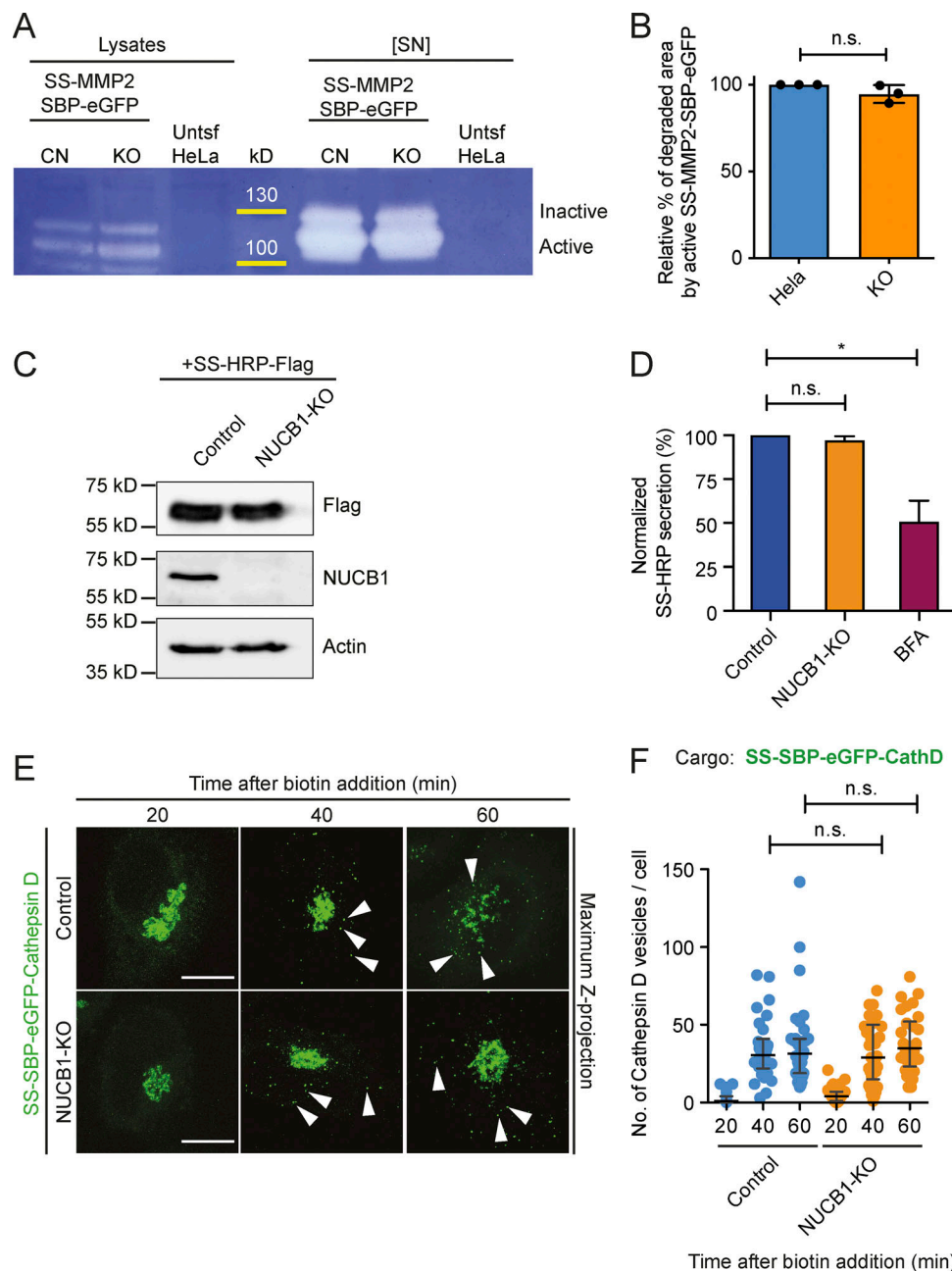


Figure S5. **NUCB1 does not affect MMP2 activation nor trafficking of other cargoes such as HRP and Cathepsin D.** (A) Zymography assay of HeLa cells expressing SS-MMP2-SBP-eGFP. Untsf HeLa, HeLa without transfection; [SN], 10 $\times$ -concentrated supernatants; CN, HeLa control; KO, NUCB1-KO. (B) Semiquantitative analysis of experiment shown in A.  $n = 3$  independent experiments; one-sample  $t$  test; n.s., nonsignificant. (C) Whole-cell lysates of HeLa and NUCB1-KO cells stably expressing SS-HRP-FLAG were analyzed by anti-FLAG, anti-NUCB1, and anti- $\beta$ -actin WB. SS-HRP-FLAG is expressed in HeLa and NUCB1-KO cells to similar levels. (D) Cell culture supernatants of cells described in C were analyzed for HRP activity by chemiluminescence after 4-h secretion. BFA served as a positive control for perturbed secretion and was added for 1 h before HRP secretion analysis. No significant differences were observed between NUCB1-KO and HeLa control cells. \*,  $P < 0.05$ . (E) HeLa or NUCB1-KO cells expressing SS-SBP-eGFP-Cathepsin D were fixed 20, 40, and 60 min after biotin addition. Representative maximum Z-projection images show Cathepsin D trafficking from Golgi to cytoplasmic vesicles (arrowheads). Scale bars, 10  $\mu$ m. (F) Quantification of cytoplasmic Cathepsin D vesicles from cells shown in E.  $n > 30$  HeLa and NUCB1-KO cells per time point; two independent experiments; mean  $\pm$  SD. Statistical analysis was performed using a nonparametric Kruskal-Wallis test with Dunn's multiple comparison test. No significant differences with  $P < 0.05$  were detected.

Provided online is one table. Table S1 lists protein candidates potentially involved in the trafficking of MMP2, found by MS.